FREQUENCY STABILIZED
GAS LASER

FINAL REPORT
Contract NAS8-20631

17 February 1967

Prepared For

National Aeronautics
and
Space Administration
Huntsville, Alabama

SYLVANIA ELECTRONIC SYSTEMS - WESTERN OPERATION
Post Office Box 205
Mountain View, California 94040

FREQUENCY STABILIZED GAS LASER
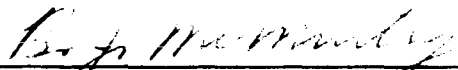
FINAL REPORT
Contract NAS8-20631

17 February 1967

R. S. Reynolds

J. D. Foster

A. A. Kamiya

A. E. Siegman

APPROVED BY: *[signature]*

Mr. M. B. Fisher, Manager
Quantum Electronic Devices Department

[signature]

Dr. B. J. McMurtry, Manager
Advanced Technology Laboratory

Prepared For

National Aeronautics and Space Administration
Huntsville, Alabama

FOREWORD

This report is the final engineering report summarizing the work performed under NASA Contract No. NAS8-20631 entitled "Frequency Stabilized Gas Laser," covering the period 17 June 1966 to 17 February 1967. This report was prepared by the Advanced Technology Laboratory of Sylvania Electronic Systems – Western Operation, Mountain View, California. It describes work performed in the Quantum Electronic Devices Department, headed by Mahlon B. Fisher. Mr. Richard S. Reynolds is the principal investigator; other major contributors are Dr. J. D. Foster, Mr. W. R. Hill, Mr. A. Kamiya, and Professor A. E. Siegman of Stanford University (consultant).

All the work performed under this contract was administered under the Astrionics Laboratory, NASA George C. Marshall Space Flight Center, Huntsville, Alabama. Dr. J. L. Randall is the principal technical representative for the laboratory.

ABSTRACT

This report covers the results of an eight-month study and design program directed toward the attainment of a frequency-stabilized, single-frequency CO_2 laser operating at a wavelength near 10.6 microns. To provide long-term stabilization, a technique which allows a CO_2 laser to be stabilized with respect to a non-regenerative CO_2 amplifier was chosen. This technique is analyzed and shown to be capable of providing a frequency stability of about 1 part in 10^{10} using presently available 10-micron detectors.

Factors affecting the absolute stability of the CO_2 amplifier frequency are discussed with the conclusion that pressure variations within the amplifier tube may be the limiting factor for long-term frequency stability.

A detailed design is presented for a CO_2 laser system capable of providing greater than 1/2 watt of 10.6 micron radiation, frequency stabilized to within 3 kHz. Techniques for ensuring single-frequency operation in the CO_2 laser without degradation in power output are also discussed.

TABLE OF CONTENTS

LIST OF TABLES

LIST OF ILLUSTRATIONS

1. INTRODUCTION

Since the discovery of the CO_2 laser in 1964, much interest has been generated for its use in applications involving communications and telemetry. The desirable combination of high efficiency (for a laser) with a high power output capability is coupled with an operating wavelength (10.6 microns) which occurs in an atmospheric "transmission window."

With these three major advantages, along with several other minor advantages associated with operation in the middle infrared (large coherence area, lower quantum noise, etc.), the necessity for the development of components suitable for operation in a sophisticated 10.6-micron system has become apparent. This program has been concerned with the techniques for developing a suitable CO_2 laser transmitter capable of being used in a heterodyne type of communication system.

The specific objectives of the program are to perform studies and develop a design toward the attainment of a CO_2 laser stabilized in frequency to 1 part in 10^{10} for an indefinite period of time in a normal laboratory environment. This figure is for both long- and short-term stabilities. Also, the laser output power shall be as high as possible consistent with the stabilization requirements and shall occur in a single frequency. This report summarizes the efforts on both the study and design phases of the program.

The laser stabilization techniques which have been used in the past[1,2,3,4] were reviewed for possible use with the CO_2 laser. These included power sensing stabilization, stabilizing to an external Fabry-Perot cavity, stabilizing by self-dispersion, Zeeman split absorption cell discrimination, ring laser techniques and stabilization by internal FM sideband generation. Many of the schemes were not found to be applicable to the CO_2 laser, and the schemes which were applicable would not entirely meet the requirements. Fortunately, a new scheme was devised for use with the CO_2 laser which can satisfy the requirements set

1

forth on the laser. It involves the technique of stabilizing the laser to an external non-regenerative CO_2 amplifier. The analysis of this scheme with sensitivity figures is presented in detail in Section 2.

Section 3 discusses the laser design requirements necessary to achieve the stability goals mentioned above. Techniques for obtaining single wavelength and single mode operation of the laser are discussed, and the most promising techniques are chosen for the detailed design. Also, the mechanical design, especially oriented toward techniques for acoustic and vibration isolation, are discussed. The servo-loop design concept is also developed in detail.

Section 4 contains concluding remarks and recommendations for further work. Section 5 is a list of references used in this report.

2. ANALYSIS OF EXTERNAL CO_2 AMPLIFIER STABILIZATION SCHEME

2.1 Introduction

The desired long-term frequency stability can clearly not be obtained by stabilization to any purely mechanical structure, but must be locked to an atomic transition, specifically to the CO_2 laser transition itself. Furthermore, it is desirable to avoid internal modulation or "dither" in the master laser oscillator, if possible. With these points in mind, we propose that the laser frequency be locked to a separate CO_2 laser amplifier, as described in more detail in this section.

Other significant advantages of this scheme include the following:

a. The master laser oscillator, since it is not the main frequency determining element, can be designed to best meet other objectives, such as power output or modulation capability.

b. The separate laser amplifier, since it need not supply any power, can have its structure, gas fill, discharge, and other parameters all adjusted for maximum long-term stability, without worrying about other performance characteristics.

c. Since the separate laser amplifier is non-regenerative, cavity pulling effects and other cavity-related disturbances are entirely absent, and only the atomic line itself is involved.

The following sections contain the analytical treatment of the scheme first for the case of a homogeneously broadened gain curve and secondly, for the more real, and difficult case of a Doppler broadened gain curve. The sensitivity functions are developed and typical operating parameters from available devices are used to estimate the sensitivity of the scheme.

2.2 The Separate CO_2 Amplifier Stabilization Scheme

The scheme to be utilized is best described with reference to Figure 1. As noted, a fraction of the main CO_2 oscillator's power output is tapped off, phase-modulated at some modulation frequency f_m, and passed through a separate CO_2 laser amplifier. A detector at the amplifier output looks for beat signals at frequency f_m and compares them with the phase modulation, the objective being to have pure FM or zero beat in the amplifier's output. A servo system controls the main oscillator's cavity length by piezoelectric tuning, in such a way as to bring the observed beat to zero.

If the main laser frequency is exactly on the CO_2 line center, then the FM sidebands are symmetrically located on the atomic line, and they remain balanced in such a fashion that there is no AM beat signal generated at the fundamental frequency f_m. If, however, the main oscillation or carrier drifts off the CO_2 line center, then the FM sidebands are asymmetrically amplified. They become unbalanced, and a fundamental beat note is generated, more or less proportional to the deviation from line center. Moreover, the phase of this beat relative to the original FM modulating signal changes sign depending on which way the drift occurs. Hence, one can identify to which side of the line the carrier has drifted.

Note that both the gain and phase shift characteristics of the inhomogeneous line are important in determining the asymmetric amplification for a signal off resonance. The long-term stability of this scheme should depend only on the long-term frequency stability of the CO_2 molecular transition itself. We will identify at the end of this section the factors that will limit or determine the long-term stability of the molecular line. The actual frequency modulation method may be electro-optic or it may be accomplished with a piezoelectrically vibrated mirror. As will be seen later, the electro-optic approach is to be preferred.

The basic elements of this stabilization scheme are the incident frequency-modulated (FM) laser signal; a single-pass laser amplifier; and a photodetector tuned to the first beat note, i.e., to the FM modulation frequency.
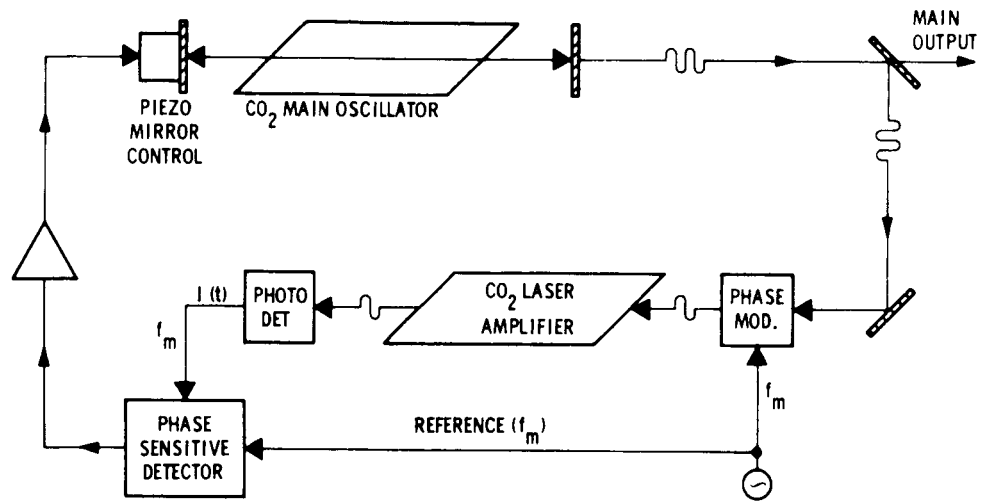
Figure 1. Schematic of the Main Control Loop.

2.3   Generation of a Beat Signal

We suppose that the incident laser beam is an FM signal with carrier frequency ω_c, modulation frequency ω_m, and FM modulation index δ, so that the incident complex amplitude $\tilde{u}_1(t)$ may be written

$$\tilde{u}_1(t) = u_o e^{j\left[\omega_c t + \delta \sin \omega_m t\right]} = u_o \sum_{n=-\infty}^{\infty} J_n(\delta)\, e^{j(\omega_c + n\omega_m)t} \qquad (2.1)$$

If the complex voltage gain of the amplifier for a sideband at frequency ω is denoted by $\tilde{g}(\omega)$, then the complex output signal from the amplifier will be

$$\tilde{u}_2(t) = u_o \sum_{n=-\infty}^{\infty} J_n(\delta)\, \tilde{g}(\omega_c + n\omega_m) e^{j(\omega_c + n\omega_m)t} \qquad (2.2)$$

The instantaneous intensity striking the output detector (and hence presumably the photocurrent from this detector) will be given by

$$I(t) = \tilde{u}_2^{\,*}(t)\, \tilde{u}_2(t) \qquad (2.3)$$

If we adopt the shorthand notation

$$\tilde{g}_n \equiv \tilde{g}_n(\omega_c) = \tilde{g}(\omega_c + n\omega_m), \qquad (2.4)$$

then the photodetector output becomes

$$I(t) = u_o^2 \sum_{n=-\infty}^{\infty} \sum_{k=-\infty}^{\infty} \tilde{g}_n \tilde{g}_k^{\,*}\, J_n(\delta) J_k(\delta) e^{j(n-k)\omega_m t}$$

$$= I_o + \frac{1}{2}\left[\tilde{I}_1 e^{j\omega_m t} + cc\right] + \frac{1}{2}\left[\tilde{I}_2 e^{j2\omega_m t} + cc\right] + \ldots \qquad (2.5)$$

where we have specifically indicated the expected dc photoresponse I_o and the complex amplitudes of the beat-frequency components at the first two multiples of the modulation frequency ω_m. The symbol cc indicates the complex conjugate.

6

Sorting out the appropriate terms then yields for the dc and the first two beat components

$$I_o = u_o^2 \sum_{n=-\infty}^{\infty} \left| \tilde{g}_n \right|^2 J_n^2 \qquad (2.6a)$$

$$\tilde{I}_1 = 2u_o^2 \sum_{n=-\infty}^{\infty} \tilde{g}_{n+1} \tilde{g}_n^* J_{n+1} J_n \qquad (2.6b)$$

$$\tilde{I}_2 = 2u_o^2 \sum_{n=-\infty}^{\infty} \tilde{g}_{n+2} \tilde{g}_n^* J_{n+2} J_n \qquad (2.6c)$$

Note that the beat amplitudes are the complex peak values, and that we may as well set the incident intensity $u_o^2 = 1$. We now consider specific forms for the gain $\tilde{g}(\omega)$, and calculate the output current terms.

2.4 Homogeneous Broadening

We will consider in this section the case of an amplifier having a homogeneously broadened atomic transition with center frequency ω_o and full homogeneous linewidth $\Delta\omega_H$. Therefore, the laser amplifier's complex gain $\tilde{g}(\omega)$ may be written

$$\tilde{g}(\omega) = \exp \left[\ln g_o \frac{1}{1+j2(\omega - \omega_o)/\Delta\omega_H} \right] \qquad (2.7)$$

where g_o is the midband voltage gain. The gain for the n-th sideband of the FM signal then becomes

$$\tilde{g}_n = \exp \left[\ln g_o \frac{1}{1+j2(\omega_c - \omega_o + n\omega_m)/\Delta\omega_H} \right] \qquad (2.8)$$

where $\omega_c - \omega_o$ is the detuning between the FM signal's carrier frequency ω_c and the atomic line center ω_o. It will be convenient to express this detuning and also the modulation frequency ω_m in normalized form by defining the dimensionless variables

$$D \equiv \frac{\text{Frequency detuning}}{\text{Full atomic linewidth}} \qquad (2.9a)$$

7

$$M \equiv \frac{\text{Modulation frequency}}{\text{Full atomic linewidth}} \qquad \qquad (2.9b)$$

In the present homogeneous case, we thus have

$$D = \frac{\omega_c - \omega_o}{\Delta\omega_H} \quad , \quad M = \frac{\omega_m}{\Delta\omega_H}$$

However, we emphasize that according to the basic definition the denominators are the full atomic linewidth, so that these denominators will become the Doppler rather than the homogeneous width when we move to the inhomogeneous Doppler case.

The gain expression now becomes

$$\tilde{g}_n(D,M) = \exp\left[\ln g_o \frac{1}{1+j2(D + nM)}\right] \qquad \qquad (2.10)$$

and we can evaluate the first three photocurrent components as functions of the parameters g_o, δ, D, and M. Figure 2 shows how the magnitudes of these photocurrents vary as a function of detuning from line center. It will be noted in particular that the fundamental beat $\tilde{I}_1$ is identically zero when $D = 0$. The magnitude of this beat current varies linearly with D in the range about $D = 0$. This beat is, of course, the output parameter that we intend to use as the discriminant, to indicate any detuning of the optical carrier ω_c from the atomic line center ω_o. Note also that the dc current I_o decreases gradually with increasing detuning, D, because the signal carrier is then moved away from the gain peak. There is also a weak second-harmonic component I_2 at frequency $2\omega_m$. This component has a more complex variation with D, and does not appear to be of utility as a frequency discriminant.

Examination of the phase $\tilde{I}_1$ shows that it changes by 180° in passing through line center, as would be expected. This discriminant beat signal reaches a maximum when the detuning reaches a value

$$D \equiv \frac{\omega_c - \omega_o}{\Delta\omega_H} \simeq 0.28$$

$|\tilde{I}_{DC}|$

POWER GAIN, $G_0 = 2.0$

MODULATION INDEX, $\delta = 0.5$

MODULATION FREQUENCY, $\omega_m = 0.1 \, \triangle\omega_H$

$|\tilde{I}_1|$

$|\tilde{I}_2|$

$\longleftarrow$ DETUNING, $D = \dfrac{\omega_c - \omega_a}{\triangle\omega_H} \longrightarrow$
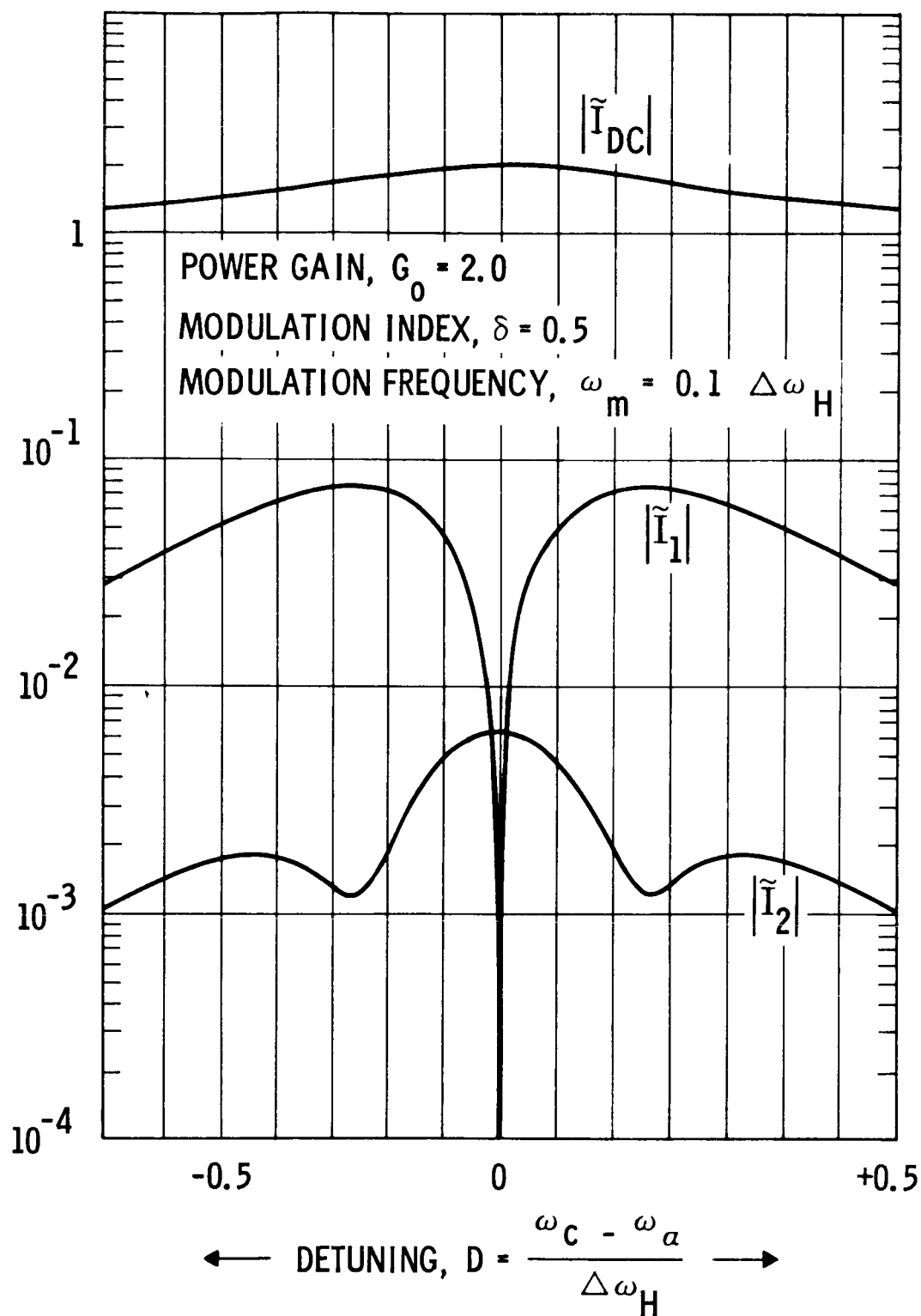
Figure 2. DC Output and Magnitude of the First Two Beat Currents
versus Detuning D for a Typical Homogeneously
Broadened Case.

and then decreases for still larger amounts of detuning. This value for the location of the maximum of $\tilde{I}_1$ is observed to remain nearly the same over wide ranges of modulation index δ and modulation frequency ω_m.

For stabilization purposes we are particularly interested in the midband sensitivity, i.e., the variation of the beat note $\tilde{I}_1$ with the detuning parameter D for small values of D. We can write for small D

$$\tilde{I}_1 \approx 2D \sum_{\eta=-\infty}^{\infty} (\tilde{g}_{n+1}\tilde{g}_n'^* + \tilde{g}_{n+1}'\tilde{g}_n^*) \; J_{n+1}(\delta)J_n(\delta) \qquad (2.11)$$

where the derivative $\tilde{g}_n'$ of $\tilde{g}_n$ in the homogeneous case is given by

$$\tilde{g}_n' \equiv \left. \frac{\partial \tilde{g}_n}{\partial D} \right|_{D=0} = -\frac{2j\ln g_o}{(1+2jnM)^2} \exp\left[\ln g_o \frac{1}{1+2jnM}\right] \qquad (2.12)$$

and both $\tilde{g}_n$ and $\tilde{g}_n'$ are evaluated at $D = 0$. From the symmetry properties of $\tilde{g}_n$ and J_n for negative n, it is easy to show that the midband sensitivity can also be written

$$\tilde{I}_1/D \approx 4 \sum_{n=0}^{\infty} (\tilde{g}_{n+1}\tilde{g}_n'^* + \tilde{g}_{n+1}'\tilde{g}_n^*) \; J_{n+1}(\delta)J_n(\delta) \qquad (2.13)$$

This expression can be easily approximated for the case of small FM modulation index, $\delta<<1$. In this case the only significant spectral components are the carrier, with $J_o(\delta) \approx 1$, and the first sidebands, with $J_1(\delta) \approx \delta/2$. The midband sensitivity can then be written

$$\frac{\tilde{I}_1}{D} \approx 4j\delta \ln g_o \left[\frac{M + jM^2}{M + j(M^2 - 1/4)}\right] e^{\ln g_o} e^{\ln g_o/(1+2jM)} , \quad (\delta<<1) \qquad (2.14)$$

The magnitude of the factor in rectangular brackets increases linearly with M for small M; passes through a maximum; and drops back asymptotically to 1 for large M. Its asymptotic and peak values are given by

10

$$
\left[\frac{M + jM^2}{M + j(M^2 - 1/4)} \right]
\begin{cases}
\simeq 4jM, & M \ll 1 \\[2ex]
= (4/3)^{1/2} \exp\left[j \arc \tan(\sqrt{2}/5) \right], & M = M_{opt} = (2)^{-1/2} \\[2ex]
\simeq 1 & M \gg 1
\end{cases}
\tag{2.15}
$$

For small δ, a modulation frequency almost as large as the atomic linewidth is obviously desirable (although an FM modulation frequency this high may not be technically feasible, especially if the modulation is accomplished with an oscillating mirror). In physical terms, the largest sideband unbalance is obtained by placing the modulation sidebands well out on the sides of the atomic line, where the gain slope $(d/d\omega)\,\chi''(\omega)$ is largest and where the phase-shifting effects $\chi'(\omega)$ are also largest.

The midband slope or _discriminant_ may thus be written for small M and δ as

$$
\left| \frac{\tilde{I}_1}{D} \right| \simeq 8M\delta\, G_o \ln G_o
\tag{2.16}
$$

where $G_o \equiv g_o^2$ is the single-pass midband power gain of the amplifier. More generally, we may write for the midband slope

$$
\left| \frac{\tilde{I}_1}{D} \right| = \left[8M\delta\, G_o \ln G_o \right] \times F(M, \delta, G_o)
\tag{2.17}
$$

where the factor $F(M, \delta, G_o)$ is unity for small M and δ, and decreases at larger values. Computer runs have shown that this factor is nearly unity over wide ranges of M and δ, as illustrated in Figure 3. It begins to fall below unity only for combinations of modulation index δ and modulation frequency M which put a significant fraction of the laser energy into sidebands falling outside the main portion of the gain curve.
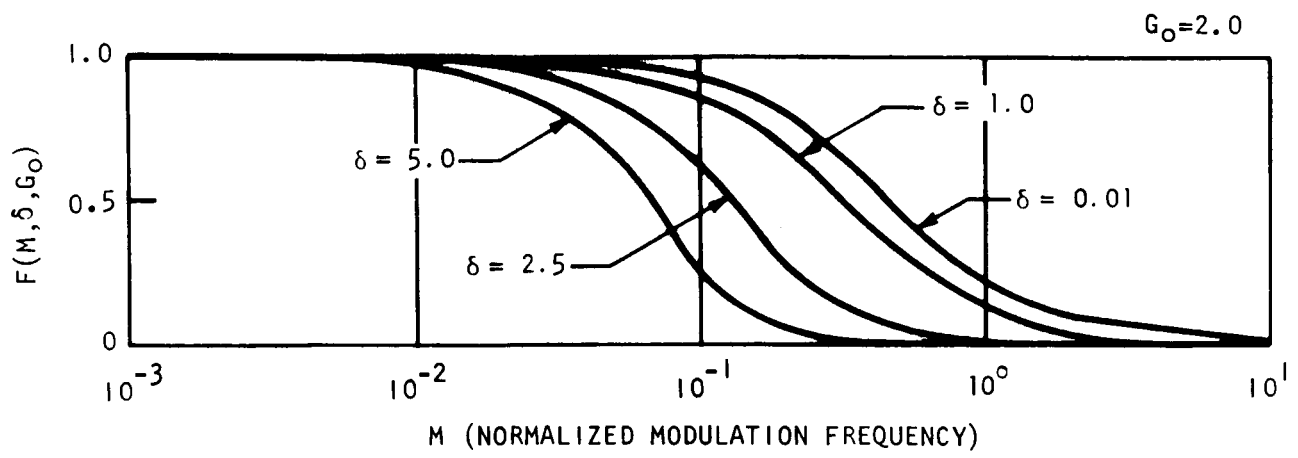
Figure 3. The Midband Discriminant Reduction Factor, $F(M, \delta, G_O)$ for Several Values of δ

2.5   Inhomogeneous (or Doppler) Broadening

We now need to consider the more realistic case of an inhomogeneously broadened atomic transition, such as is characteristic of Doppler-broadened gas lasers. The gain in this case may be written

$$\tilde{g}(\omega) = \exp\left[-j \frac{1}{2} kL \, \tilde{\chi}(\omega)\right] \tag{2.18}$$

Here k is the propagation constant neglecting any atomic interaction; L is the amplifier length; and $\tilde{\chi}(\omega)$ is the complex atomic laser susceptibility, given by

$$\tilde{\chi}(\omega) = j\chi_o'' \, \frac{2}{\Delta\omega_D} \, \sqrt{\frac{\ln 2}{\pi}} \, \int_{-\infty}^{\infty} \frac{1}{1 + 2j(\omega-\omega_o')/\Delta\omega_H} \; \exp$$

$$\left[-\left(\frac{2\sqrt{\ln 2}}{\Delta\omega_D}\right)^2 (\omega_o' - \omega_o)^2\right] d\omega_o' \tag{2.19}$$

In this expression $j\chi_o''$ is the midband susceptibility of a single homogeneous line or "spectral packet" having homogeneous linewidth $\Delta\omega_H$. The first factor inside the integral gives the frequency variation of $\chi(\omega)$ for a single homogeneous packet centered at ω_o' . The second (exponential) factor gives the distribution of packet center frequencies ω_o' about the line center ω_o , with Doppler linewidth $\Delta\omega_D$.

If we use the same basic definitions for normalized detuning and normalized modulation frequency as above, we will now have

$$D \equiv \frac{\text{Frequency detuning}}{\text{Atomic (Doppler) linewidth}} = \frac{\omega_c - \omega_o}{\Delta\omega_D} \tag{2.20a}$$

$$M \equiv \frac{\text{Modulation frequency}}{\text{Atomic (Doppler) linewidth}} = \frac{\omega_m}{\Delta\omega_D} \tag{2.20b}$$

13

Note that $\Delta\omega_H$ is now replaced by $\Delta\omega_D$ in these definitions. We also define the homogeneous broadening parameter

$$H \equiv \frac{\text{Homogeneous linewidth}}{\text{Inhomogeneous linewidth}} = \frac{\Delta\omega_H}{\Delta\omega_D} \qquad (2.20c)$$

The laser susceptibility expression, evaluated at a sideband frequency $\omega = \omega_c + n\omega_m$, may now be written

$$\tilde{\chi}(\omega=\omega_c+n\omega_m) = jH\chi_o'' \sqrt{\frac{\ln 2}{\pi}} \int_{-\infty}^{\infty} \frac{1}{\sqrt{\ln 2}\ H + 2j(D+nM) - jy} e^{-y^2} \, dy$$

$$= jH\chi_o'' \sqrt{\frac{\ln 2}{\pi}} \ \tilde{K}\left(\sqrt{\ln 2}\left[H + 2j(D+nM)\right]\right) \qquad (2.21)$$

where we define the new function

$$\tilde{K}(\tilde{\alpha}) \equiv \int_{-\infty}^{\infty} \frac{1}{\tilde{\alpha} - jy} e^{-y^2} \, dy \qquad (2.22)$$

The argument $\tilde{\alpha}$ of this function will, in general, be complex. The problem now reduces to evaluating the rather complicated function $\tilde{K}(\tilde{\alpha})$; we will give various series expansions for $\tilde{K}(\tilde{\alpha})$ shortly.

The gain seen by a sideband at $\omega = \omega_c + n\omega_m$ in an inhomogeneous line can now be written

$$\tilde{g}_n(D,M,H) = \exp\left[\ln g_o \frac{\tilde{K}\left(\sqrt{\ln 2}\left[H + 2j(D+nM)\right]\right)}{\tilde{K}(\sqrt{\ln 2}\ H)}\right] \qquad (2.23)$$

We also will need the derivative of this gain with respect to D , evaluated at $D = 0$, which takes the form

$$\tilde{g}_n'(M,H) = 4j\sqrt{\ln 2}\ \ln g_o \frac{\tilde{\beta}_n \tilde{K}(\tilde{\beta}_n) - \sqrt{\pi}}{\tilde{K}(\sqrt{\ln 2}\ H)} \exp\left[\ln g_o \frac{\tilde{K}(\tilde{\beta}_n)}{\tilde{K}(\sqrt{\ln 2}\ H)}\right] \qquad (2.24)$$

14

where $\tilde{\beta}_n$ is the combination

$$\tilde{\beta}_n \equiv \sqrt{\ln 2} \ (H + 2jnM) \tag{2.25}$$

These expressions for $\tilde{g}_n$ and $\tilde{g}_n'$ may now be used to compute the output signal from the laser amplifier.

In the present case extensive calculations carried out for wide ranges of M, D, H and δ would be largely academic. As a practical matter we are concerned with values << 1 for all of these variables. Within this degree of approximation we can expand $\tilde{K}(\tilde{\alpha})$ in the form (see Appendix A)

$$\tilde{K}(\tilde{\alpha}) \approx \pi - 2\sqrt{\pi}\tilde{\alpha} \quad , \quad |\tilde{\alpha}| << 1 \tag{2.26}$$

and the series expansion for the beat signal $\tilde{I}$, can also be expanded, in the same manner as was done for the homogeneous case. The result of this approximation is

$$\tilde{I}_1 \approx - (8 \ln 2) \ (G_o \ \ln G_o) \ MD\delta \tag{2.27}$$

Hence the midband slope or discriminant is

$$\frac{|\tilde{I}_1|}{D} \approx - (8 \ln 2) \ (G_o \ \ln G_o) \ M\delta \tag{2.28}$$

Note that this is exactly the same, except for a minor numerical difference, as the homogeneous result. The homogeneous linewidth parameter H drops out entirely -- as might be expected since no saturation phenomena are taking place. By analogy with the homogeneous case we may expect this expression to remain valid for a wide range of values of G_o , M , and δ.

2.6   Calculation of System Sensitivity

In this section we calculate the sensitivity of the FM amplifier frequency stabilization method assuming a real infrared detector, with its many performance limitations.

From our previous analysis we have found that the peak value of the modulation-frequency beat Note I, is related to the input beam intensity I_o , the detuning factor D , and other parameters by

$$I_1 = (8 \, \ell n \, 2) \, (G_o \, \ell n \, G_o) \, I_o MD\delta \tag{2.29}$$

If we use a photoconductive IR detector with a responsivity R (measured in volts/watt), the rms <u>signal voltage</u> V_s from the detector at the modulation frequency will be

$$V_s = \frac{1}{\sqrt{2}} \, RI_1 \tag{2.30}$$

If we express I_1 in terms of the modulation frequency f_m , Doppler linewidth at half height Δf_D , and detuning $\Delta f = f_c - f_o$, this becomes

$$V_s = (4\sqrt{2} \, \ell n \, 2) \left[\frac{(G_o \, \ell n \, G_o) \, RI_o f_m \delta}{\Delta f_D^2} \right] \Delta f \tag{2.31}$$

$$= \frac{4(G_o \, \ell n \, G_o) \, RI_o f_m \delta}{\Delta f_D^2} \Delta f$$

The signal voltage is, of course, linear in the frequency detuning or frequency error Δf.

The rms <u>noise voltage</u> V_n from an IR detector within a detection bandwidth B can be related to the specified responsivity R and noise equivalent power (NEP) of the detector by

$$V_n = R \times NEP \times \sqrt{B} \tag{2.32}$$

where the NEP is specified by the detector manufacturer assuming a 1 Hz detection bandwidth. The noise voltage can also be written in terms of the detector area A and the specified D* of the detector, in the form

$$V_n = \frac{R\sqrt{A}\sqrt{B}}{D*} \tag{2.33}$$

16

In using these expressions one must be careful to use values of R , NEP and $D*$ all determined for the same experimental conditions.

If we combine the above expressions for V_s and V_n we can obtain the signal-to-noise ratio in the form

$$\frac{V_s}{V_n} = \frac{4(G_o \ln G_o) I_o f_m \delta}{NEP \sqrt{B} \Delta f_D^2} \Delta f \tag{2.34}$$

Suppose that we take as the minimum detectable signal criterion a signal-to-noise ratio of unity. Then, the minimum detectable frequency error $(V_s/V_n = 1)$ for the real IR detector case is given by

$$\Delta f_{min} = \frac{NEP \sqrt{B} \Delta f_D^2}{4(G_o \ln G_o) I_o f_m \delta} \tag{2.35}$$

or, alternatively,

$$\Delta f_{min} = \frac{\sqrt{A} \sqrt{B} \Delta f_D^2}{4D*(G_o \ln G_o) I_o f_m \delta} \tag{2.36}$$

Our next step is to put realistic numbers into these expressions.

Certain parameters in the experiment are fairly firmly determined. For example, the maximum gain in a CO_2 laser amplifier is known to be approximately 40% per meter.

Therefore, by constructing a simple optical system to provide, say, triple pass of the optical beam through a 60-cm long amplifier tube, the gain would be

$$G_o \approx 2.0$$
$$\ln G_o \approx .693$$

$\left.\right\}$ $L = 60$ cm, 3 passes.

17

Also, the Doppler linewidth in a CO_2 laser is well established

$$\Delta f_D \approx 45 \text{ MHz} .$$

The detector parameters depend, of course, on the detector chosen. One IR detector that is available, fairly simple, and requires only liquid nitrogen cooling, is the Philco GPC-215. The important parameters of this gold-doped germanium photoconductor are summarized in Table I. The important number for our purposes here is

$$\text{NEP} \ (\lambda = 10.6 \ \mu) \approx 8.3 \times 10^{-11} \ \text{watt}/\sqrt{\text{Hz}}$$

This value is estimated by extrapolation, but is believed to be fairly reliable.

System parameters are somewhat subject to our design control, and must be chosen within feasible ranges. We will specify, for example, a modulation frequency of

$$f_m = 1 \text{ MHz} = 10^6 \text{ Hz}$$

It is proposed that the modulator should be of the electro-optic type, using GaAs (See Section 3). Modulation of 10.6 micron radiation using this material has been demonstrated with good performance. We suppose that a reasonable modulation index will be

$$\delta = 1 \text{ radian}$$

Table I.   PHILCO GPC-215 INFRARED DETECTOR
P-Type Ge:Au Photoconductor
$A = 2.5 \times 10^{-3} \text{ cm}^2$ $T = 77°K*$

Parameter	$\lambda = 5.5 \ \mu$	$\lambda = 10.6 \ \mu**$
Responsivity R***	14×10^3 volts/watt	7×10^2 volts/watt
Detectivity D*	6×10^9 cm$\sqrt{\text{Hz}}$/watt	3×10^8 cm$\sqrt{\text{Hz}}$/watt
NEP	4.2×10^{-12} watt/$\sqrt{\text{Hz}}$	8.3×10^{-11} watt/$\sqrt{\text{Hz}}$

Notes: *   Performance is significantly improved if the operating temperature is reduced to $T = 65°K$

   **   Values for $\lambda = 10.6$ microns are estimated by slight extrapolation of published curves.

   ***   At ~100 μa bias. Responsivity varies linearly with bias, while D* and NEP remain very nearly unchanged.

The detection bandwidth is more or less arbitrarily chosen as

$$B = 100 \text{ Hz}$$

This is a compromise between sensitivity and speed of response.

We have finally to choose the total intensity I_o incident on the detector. The manufacturer specifies that for 500°K blackbody radiation the GPC-215 is linear to signal levels I_o (500°K) $\geq 10^{-6}$ watts, with a responsivity to this radiation of R(500°K) $\simeq 7 \times 10^3$ volts/watt. This implies linear response up to signal voltages of at least $V_s = 7 \times 10^{-3}$ volts. In fact, since the bias voltage on the detector is approximately 20 volts in normal operation, it seems safe to assume that the signal voltage could go at least as high as 0.2 volts without too much departure from linearity. (The manufacturer also specifies no damage from, and very rapid recovery from, even "massive radiation overloads").

Our chief problem is that the desired beat signal I_1 rides on top of a very large dc input I_o , and the dc response of the detector to I_o is the limiting factor. It seems reasonable to assume that we can operate with an input I_o at 10.6 microns which, when multiplied by the 10.6 micron responsivity, causes a dc signal voltage of less than 0.2 volts. Therefore, we specify

$$I_o \ (10.6 \ \mu) = \frac{0.2 \text{ volt}}{R(10.6 \ \mu)} \tag{2.37}$$

$$= \frac{2 \times 10^{-1} \text{ volt}}{7 \times 10^2 \text{ volt/watt}}$$

$$= 280 \ \mu \text{ watt}$$

This is certainly well within the available power from the laser amplifier.

If we combine all of the above numbers, the final result for the minimum detectable frequency error is

$$\Delta f_{min} \simeq 1.1 \times 10^3 \text{ Hz} \tag{2.38}$$

The fractional frequency stability which this number represents is

$$\frac{\Delta f_{min}}{f_o} = \frac{4.3 \times 10^4}{3 \times 10^{13}} = 3.5 \times 10^{-11} \qquad (2.39)$$

Therefore, this value achieves the objective of 1 part in 10^{10} frequency stability.

We have, however, deliberately chosen values for all of the system parameters which were not pushed to their maximum values, in order to obtain a fairly realistic estimate. In Table II, we have tabulated both these somewhat conservative design choices, and also the results of a reevaluation using a "stretched" set of system parameters. The result with the stretched parameters is

$$\Delta f_{min} = 4 \text{ Hz} \qquad (2.40)$$

and hence a frequency stability of

$$\frac{\Delta f_{min}}{f_o} = 1.3 \times 10^{-13} \qquad (2.41)$$

This result is not to be taken as a design prediction, but is only intended to show that with some optimizing of the system parameters extremely good stabilities are feasible.

There also appear to be some "safety factors" which are available to compensate for any overly optimistic assumptions in our choices of parameters. These "safety factors" can be invoked if and when required to compensate for any other unforeseen difficulties. A list of possible "safety factors" includes:

1) If detector performance is a seriously limiting factor, it is possible to go to a helium-cooled detector, thereby gaining greatly improved detectivity (at a considerable cost in practical convenience). Typically these detectors will offer about a factor of 20 reduction in NEP.

20

Table II. ESTIMATION OF MINIMUM FREQUENCY ERROR

$$\Delta f_{min} \simeq \frac{NEP \sqrt{B} \; \Delta f_D^2}{4(G_o \; \ell n \; G_o) \; I_o f_m \delta}$$

Parameter	Initial Design	"Stretched" Design
Detector NEP	$8.3 \times 10^{-11} \frac{Watts}{(Hz)^{1/2}}$	$5 \times 10^{-11} \frac{Watts}{(Hz)^{1/2}}$
Detection Bandwidth B	100 Hz	1 Hz
Doppler Linewidth Δf_D	45 MHz	40 MHz
Laser Gain G_o	2.0	2.0
Laser Power I_o	0.28 mw	1 mw
Modulation Frequency fm	1 MHz	4 MHz
Modulation Index δ	1	1
Minimum Frequency Error Δf_{min}	1.1 kHz	4 Hz
Frequency Stability $\Delta f_{min}/fo$	3.5×10^{-11}	1.3×10^{-13}

2) <u>Cooling the walls</u> of the CO_2 laser amplifier will reduce the Doppler width Δf_D, and probably also increase the available gain G_o.

3) The performance of the simpler nitrogen-cooled detectors should be capable of at least some improvement, by <u>limiting the field of view</u> to the very small angle needed for this application; optimizing the choice of <u>window material</u>; optimizing the detector <u>geometry</u>; and pumping on the nitrogen to cool <u>below 77°K</u>.

4) Concentration on modulator design and optimization should permit either <u>higher modulation frequency</u> f_m (if detector limitations permit), and/or substantially <u>higher modulation index</u> δ.

5) Use of the detector as a <u>combined photodetector</u> and modulation-frequency <u>mixer</u>, by using rf detector bias, will permit higher modulation frequencies, and may also improve noise performance.

6) Even higher values of the power I_o from the CO_2 amplifier may be usable, especially with rf bias. The usable response range of available detectors should be checked early in future experimental programs.

2.7 Second-Order Frequency Shifts in CO_2 Laser Amplifiers

When one's objective is high-frequency stability, consideration of first-order frequency shifts is not sufficient, and one must be prepared to closely examine more difficult second-order effects that will have an effect on the oscillation frequency. We now consider some of these effects.

2.7.1 Discharge Conditions: Pressure and Temperature Broadening and Shifts

For the case of a frequency stabilized laser, one will want to carefully stabilize the discharge conditions, the pressure, and the wall temperature in the laser proper. It is not possible at this point to predict the sensitivity

to these parameters in detail, and this will form one aspect of the development program. However, we can carry out some very rough estimates, as follows.

The dominant source of inhomogeneous broadening in the CO_2 laser is the random Doppler broadening arising from the random thermal velocities of the CO_2 molecules. The full linewidth Δv_D of any transition due to Doppler broadening is $\Delta v_D \approx 50$ MHz for the 10.6-micron CO_2 transitions.

However, there will also be both a certain amount of homogeneous line broadening Δv_L and a transition frequency shift Δv_S resulting from collisions of CO_2 molecules with other gas atoms and with each other. The broadening is called Lorentz broadening, or by some, Holtzmark broadening where it is due to collisions to an atom with other atoms of the same kind. There is a standard kinetic theory expression for the number of collisions per second (per unit volume) in a mixture of gases of types 1 and 2, namely,

$$Z = 2N_1N_2\sigma^2 \sqrt{2\pi kT\left(\frac{1}{M_1} + \frac{1}{M_2}\right)} \qquad (2.42)$$

Where N_1 and N_2 are the concentrations of the two types, and M_1 and M_2 are the molecular masses. The parameter σ^2 is the effective cross-section for the process; typical values of this parameter are $\sigma^2 \approx (20 - 80) \times 10^{-16}$ cm^2. Gerry and Leonard have recently measured this quantity to be 57×10^{-16} cm^2 for CO_2 molecules.[5] If Z is the total number of collisions in unit volume, the average number of collisions per unit time for a single molecule is

$$Z_L = \frac{Z}{N_1} \qquad (2.43)$$

The full linewidth Δv_L due to Lorentz or collision broadening is then given by

$$\Delta v_L = \frac{Z_L}{\pi}$$

$$= \frac{2}{\pi} N_2\sigma^2 \sqrt{2\pi kT\left(\frac{1}{M_1} + \frac{1}{M_2}\right)} \qquad (2.44)$$

This says that the Lorentz broadening of a transition in molecules of type 1 is directly proportional to the concentration (or pressure) N_2 of any other gas of type 2; and this can be experimentally verified. At the same time, by simply changing N_2 and M_2 to N_1 and M_1 one can get a reasonable idea of the Lorentz (or Holtzmark) broadening resulting from self-collisions with molecules of the same kind. Putting rough numbers into the expression above gives

$$\Delta\nu_L \approx 1 - 10 \text{ MHz per Torr} \tag{2.45}$$

as the amount of Lorentz or collision broadening for a given gas pressure. The higher figure, that is, ~10 MHz per Torr , seems to be close to correct for CO_2, so that at a pressure of several Torr the homogeneous linewidth of the CO_2 vibrational transitions is several tens of MHz.

Other measurements by Gerry and Leonard indicate that the cross-sections for collisions of CO_2 and N_2 or CO are nearly the same as for collisions of CO_2 with itself; i.e., $\sigma^2 \approx 50$ to $56 \times 10^{-16} \text{cm}^2$. The cross-section against He seems to be noticeably smaller, $\sigma^2 \approx 18 \times 10^{-16} \text{ cm}^2$.

There is also a Lorentz shift in the line center frequency resulting from collisions, which causes the overall line to be shifted to lower frequencies. This shift results because when two molecules come near each other, the transition frequencies of either molecule tend to be pulled downward because of the nature of the Franck-Condon potential-vs-radius curves. If every molecule undergoes occasional collisions, its transition frequencies tend on the average to be pulled slightly lower in frequency, since the molecule spends some fraction of its time near other molecules.

The theory of this shift is very involved, but the net result is that the Lorentz shift $\Delta\nu_S$ and the Lorentz broadening $\Delta\nu_L$ are related by

$$\frac{\Delta\nu_S}{\Delta\nu_L} \approx 0.2 - 0.4 \tag{2.46}$$

in many gases. Actually, we have some data on the pressure shift in CO_2.
Patel notes that CO_2 laser wavelengths, measured at less than 1 Torr,
are shifted from earlier CO_2 wavelengths measured in absorption or spon-
taneous emission at 1 atmosphere (760 Torr) by about 0.17 cm^{-1} = 5.1 x 10^9 Hz.
This corresponds to a pressure shift

$$\frac{\Delta \nu_S}{P} \approx \frac{5 \times 10^9 \text{ Hz}}{760 \text{ Torr}} \approx 6.6 \frac{\text{MHz}}{\text{Torr}} \qquad (2.47)$$

Since an optimum CO_2 laser discharge will contain perhaps a few Torr of other
gases such as N_2 and He, in addition to the CO_2, it appears that very careful
pressure (and temperature) control will be necessary in order to eliminate
frequency shifts due to pressure variations.

2.7.2 Isotope Shifts

Naturally occurring oxygen has two isotopes O^{14} and O^{15}, with natural
abundances of 99.63 percent and 0.37 percent, respectively, while the
common natural isotopes of carbon are C^{12} (98.89 percent) and C^{13} (1.11
percent). Therefore, one needs to consider possible line shifts and/or
asymmetries because of isotope shifts, such as are well known in He-Ne
lasers.

Actually, the isotope shifts in vibrational-rotational bands are quite
large, because the changed mass of the nucleus significantly changes both
the vibrational frequency and the rotational moment of inertia. For
instance, the isotope shift in one of the transitions involved in the laser
action between $C^{12}O_2^{16}$ and $C^{13}O_2^{16}$ is ~3 percent. Hence, the isotopically
shifted components are probably moved entirely outside the frequency range
of interest, and we can probably ignore completely any effects because of
the very small natural concentrations of C^{13} and O^{15}.

2.7.3 Zeeman Shifts

Each of the J rotational levels of the CO_2 molecule is still (2J + 1)
fold degenerate (space degeneracy) because of the multiple allowed orienta-
tions of the angular momentum vector in space. Application of a dc

25

magnetic field B_0 will cause this degeneracy to be lifted. Each J level, and its associated transitions, will be split into $2J + 1$ components.

The amount of this Zeeman splitting between two adjacent components can be written as

$$\Delta f = g_J(\beta/h)B_0 \qquad (2.48)$$

where β is the nuclear magneton, and g_J is a numerical factor, called simply "the g value", (or the spectroscopic splitting factor). For a single nuclear spin, for example, g_J has the value 2.0, and the levels split at the rate $\Delta f/B_0 \approx 1.5$ kHz/gauss.

However, the magnetic dipole moment produced by a rotating molecule is relatively small, because both the positive nuclear charges and the negative electron cloud rotate around together. Thus, the net circulating current and the associated magnetic dipole moment are small. While detailed g_J values for the CO_2 levels are not available, typical values for rotating molecules are

$$g_J \approx 0.02 - 0.05 \qquad (2.49)$$

Therefore, the Zeeman splitting rate is

$$\frac{\Delta f}{B_0} \approx (0.02 - 0.05) \frac{\beta}{h} \qquad (2.50)$$

$$\approx (15 - 35) \frac{Hz}{gauss}$$

It should be easy to keep ambient magnetic fields well below 1 gauss. In any case, the first-order effect of the Zeeman effect will be simply to broaden the CO_2 lines very slightly, since the lines split symmetrically with components being shifted both upwards and downwards. Hence, it does appear that Zeeman effects should not be a serious obstacle to good frequency stability.

2.7.4 Stark Effect Shifts

There are possibly dc and rf electric fields present in the CO_2 laser, and hence the possibility of Stark frequency shifts in the CO_2 line must be considered. However, it appears that any Stark perturbations will, in fact, be extremely small. First, because the CO_2 molecule has no permanent electric dipole moment, there will be no first-order Stark effect, but only a second-order effect in which the splitting goes as E_0^2 for small electric fields E_0 . Secondly, Stark splitting decreases rapidly with increasing J values, and CO_2 lasers operate on relatively large-J transitions, e.g., P(20). Thirdly, both upper and lower laser levels may be shifted in the same direction, so that their difference may be very little changes.

By examining the limited data available on second-order Stark splitting of molecular levels, we conclude that Stark shifts due to the discharge fields should not be a problem.

3.0   DESIGN OF FREQUENCY-STABILIZED CO_2 LASER

3.1   Introduction

To obtain the desired goals of 1 part in 10^{10} frequency stability, two uniquely different stabilization techniques must be used. As was pointed out in Section 2, the bandwidth of the servo-loop must be kept to less than 100 Hz in order to reduce the system noise to the point where a frequency deviation from the CO_2 amplifier of $1:10^{10}$ can be detected. The external amplifier or electronic scheme then will only be able to provide essentially "long-term" stabilization. Then, to reduce frequency fluctuations which may occur at higher rates than 100 Hz, the laser must be isolated from the acoustical and vibrational world around it so as to eliminate any effects which would normally cause frequency "jitter." From a system viewpoint, the latter is a more severe problem since in many applications involving heterodyne communications, the long-term frequency drifts can be tracked out by the system local oscillator, leaving the short-term fluctuations to add noise to the signal. In this case the mechanical package must be designed to reduce the effects of the normal acoustical environment in which the laser must operate if satisfactory "short-term" frequencies are to be obtained.

Therefore, great attention must not only be paid to the analysis and evaluation of the electronic scheme for stabilization, but techniques must be developed to obtain the necessary mechanical rigidity and stability consistent with the peculiarities of the CO_2 laser.

For the low frequency or long-term stabilization, the laser output is compared to a fixed frequency, determined by the CO_2 molecular transition itself in the amplifier, and adjusted to match the amplifier frequency. The technique for generating the error signal was discussed in Section 2. Figure 4 is a block diagram of the electrical stabilization system including the laser excitation power sources.
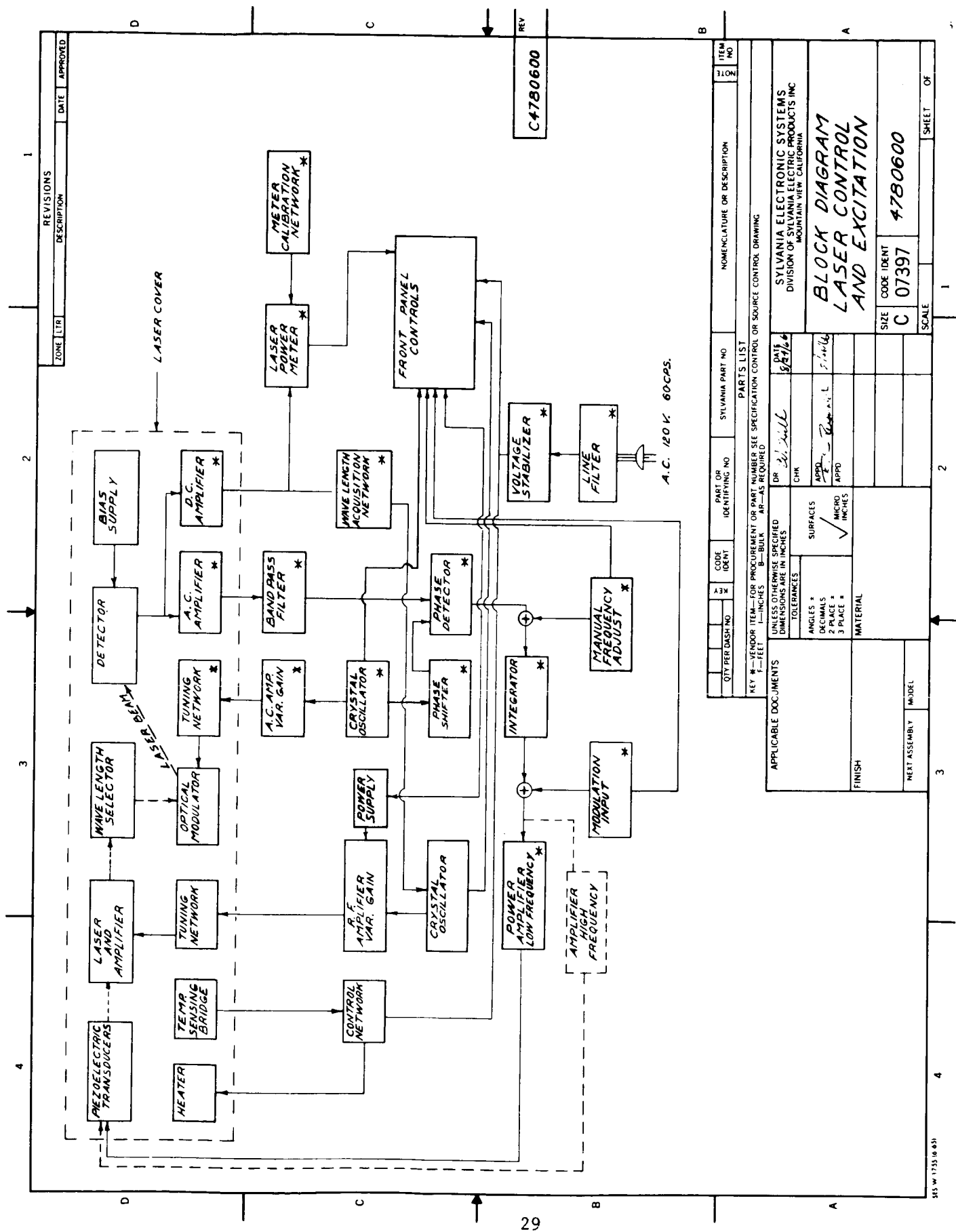
Figure 4. Block Diagram Laser Control and Excitation.

To obtain the desired error signal, the control system frequency modulates a small portion of the main laser beam at a modulation frequency f_m (in this case $f_m \approx 1$ MHz) with an optical modulator. The modulated beam is then amplified in a control laser amplifier which has a gain profile determined only by the atomic gain profile of the CO_2 transition. When the distorted frequency modulated signal, the main laser signal being off the atomic line center, is amplified, unequal amplitudes and phases of the opposite sidebands cause an unbalanced condition resulting in generation of a beat at the modulation frequency. The amplitude of the beat is proportional to the amount of frequency drift, while the phase of the beat reverses at the frequency corresponding to the atomic line center. The wavelength selector ensures that the laser will operate only on a preselected wavelength . The frequency stabilization control system processes this beat signal and produces a suitable signal necessary to drive the piezoelectric tuning device. The tuning device, in turn, controls the optical cavity length causing the FM carrier frequency to lie at the atomic line center of the CO_2 amplifier.

The modulated laser signal is detected by the low noise photodetector, located within the laser housing, which converts it to a processable electrical signal. The low-noise, high-gain amplifier circuit amplifies and band-limits the modulated signal such that the signal can be phase detected by the phase detector. Since the sensitivity of the stabilization control system is essentially governed by the abilities of the photodetector to detect a very weak signal, at f_m, riding on top of a large dc signal from the laser, and the bandpass amplifier to amplify the small detected signal, the noise figures of these devices become a limiting factor to the degree of frequency stabilization the system can achieve.

The sidebands of the photodetector output signal contain information relating to frequency perturbations caused by thermal drift, and acoustical and thermal noise on the laser output. These perturbations, after an amplification, are detected to a low-pass spectrum by the phase detector operating at the 1 MHz carrier frequency.

The low-frequency, phase detected signal then is filtered, frequency compensated, integrated and amplified to produce correction signals for driving the piezoelectric tuning device. The integrator performs an integration of the error signal, thereby reducing the dc component of the error signal to zero. The dc high voltage driver amplifies the error signal to the level suitable for driving the tuning device. The closed-loop servo bandwidth of the control system is approximately 100 Hz.

The function of the wavelength acquisition circuit is to generate a series of repetitive triggering pulses when the main laser runs on an incorrect wavelength. The triggering pulses are fed to the laser power supply unit for restarting the laser oscillator until the laser runs on the correct wavelength. A calibrated power meter indicates the output power level of the laser.

The temperature inside the laser enclosure at the laser cavity is controlled by the temperature control circuit. It is expected that the temperature inside the enclosure can be stabilized to about $\pm 1^{\circ}C$ utilizing a thermistor-actuated bridge network.

As an added convenience, although not necessary for this application, a modulation input jack is provided so that external frequency modulation can be applied to the laser via the piezoelectric transducer. Also, a manual frequency adjust bias circuit is included so that the frequency of one laser can be offset by some desired amount from another similar laser during heterodyne tests to provide a convenient intermediate frequency.

Shown in dotted lines is a portion of the feedback system which may be included at a later date. As new photodetectors become available with lower noise characteristics, it may be possible to increase the bandwidth of the servo-loop. To take advantage of the increased bandwidth, it appears most advantageous to include a separate high-frequency circuit with a special high frequency - low amplitude piezoelectric transducer. This transducer would be chosen to complement the original low frequency - large amplitude transducer.

31

In order to reduce electrical drifts and high-frequency noise due to the electrical power source, a voltage stabilizer and low-pass line filter will be necessary in the power line. The front panel will house only the required controls for normal operation of the laser system.

Within the size limitation imposed on the laser head (1 meter cube), a layout has been made of the section within the "laser cover" shown on the block diagram. The laser plan view is depicted in Figure 5, showing the relative positions of each of the individual assemblies. The length of the entire unit is 100 cm and the width is 37 cm. Its height will be 20 cm. The entire unit is surrounded by two independent acoustical damping enclosures to reduce the amplitude of airborne vibrations. The base is a special acoustical damping laminate of several relatively independent but rigid layers. Although not shown on this assembly drawing, the laser cavity itself is also isolated from the rest of the unit by acoustical damping materials. In order to maintain relatively high resonant frequencies in the laser cavity structure, the length of the cavity has been limited to 50 cm. If it is found desirable, there has been left room for lengthening the laser cavity in order to obtain higher powers. The Brewster angle laser tube (approximately 40 cm long) is potted in place within the channel-shaped invar cavity. The diffraction-coupled output mirror, shown on the left of the cavity assembly, is rigidly mounted to the cavity structure. Simple spring-type mirror adjustments have been eliminated to reduce vibration effects. The opposite mirror is non-transmitting and is mounted on the large piezoelectric transducer.

The output beam, being donut-shaped, is collimated by a cassegranian system and passed out of the laser unit through a beam splitter and a window which serves to hermetically seal the laser box. It is expected that this particular laser will provide a minimum of 500 milliwatts of stable single-frequency laser power.
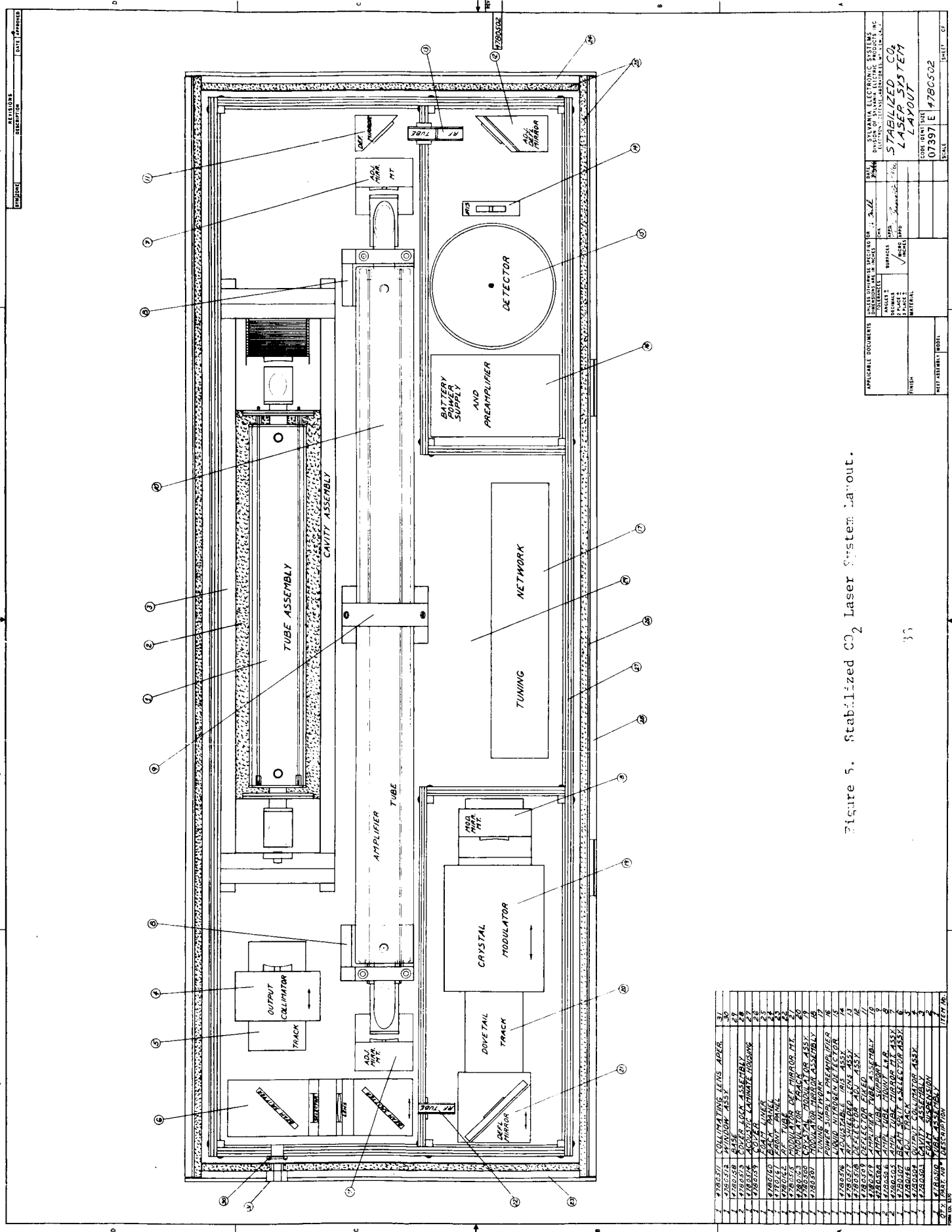
Figure 5. Stabilized CO$_2$ Laser System Layout.

The output beam splitter will provide about 10 - 20 milliwatts to the stabilization network which comprises the rest of the components in the assembly. The low level control beam is passed through a Fabry-Perot type of wavelength selector adjusted to have transmission only at the desired wavelength. After passing through a converging lens and a low-pass beam splitter, the beam is brought to the optical modulator. The active element of the optical modulator is a GaAs crystal 3 mm square and about 8 cm long. The optical beam is double-passed in the modulator by the beam-folding mirror attached to the back of the modulator housing. The entire modulator assembly is enclosed in an electrically-tight box, to reduce any stray pickup by the detector at the modulation frequency.

After passing through the modulator twice, the beam is brought back to the second beam splitter and enters the CO_2 amplifier tube. In order to obtain the desired gain in the amplifier, the amplifier is triple-passed by the entering beam. The mirror curvatures and aperture hole sizes are chosen to maximize gain without allowing the amplifier to oscillate. The amplified CO_2 laser beam is then brought into the detector area through an RFI enclosure and is optically matched to the size of the detector. A battery-controlled bias circuit and first-stage amplifier at f_m are within the detector enclosure to decrease noise pickup. The detector will require liquid nitrogen cooling by liquid transfer so that a fill port will be made available through the acoustical covers to the outside of the package. The RFI enclosure around the detector will also be constructed as an acoustical attenuator.

In order to maintain stability of the pressure and gas composition in the laser and especially in the CO_2 amplifier, a non-flowing, sealed-off system is necessary. To preserve long lifetimes, the laser and amplifier will be excited with RF energy. A matching network is located within the laser enclosure to match the output from a standard RF exciter to the required laser and amplifier impedances. It is expected that about 100 watts of RF power will be necessary.

34

The following sections describe in more detail the major individual assemblies and electrical components. The mechanical design concepts on the thermal and acoustical problems are presented, along with the results of the studies and designs for the optical and electrical system. Also, because of the importance of the detector in the stabilization scheme, a short section contrasting several 10-micron detectors is included.

3.2 Characteristics of Several Photoconductive Detectors Usable at 10.6 Microns

At present, the types of detectors usable at 10.6 microns fall into two categories, thermal and photoconductive. The thermal detectors are useful for determining average power levels but cannot respond to intensity changes much beyond about 100 cps. The photoconductive detectors, however, can have a much higher frequency response extending into the high megahertz range. For communication or heterodyne purposes, the photoconductive detectors are the only readily available type for 10.6-micron radiation.

The most notable photoconductive detectors for use at 10.6 microns are compared in Table III. Except for the Ge;Au types, these detectors can have peak quantum efficiencies in the 20-to-50 percent range, much closer to an ideal detector than photoelectric devices.

For the Hg-, Cu-, and Zn-doped detectors, the operating temperature indicated in the table is at, or slightly below, that required to reach a condition of background $(T = 300^{\circ}K)$ limited operation.

Except for the gold-doped detectors, these materials respond into the infrared beyond the 10.6-micron wavelength with good sensitivity. The black body peak response for the Hg:Cd:Te and the Ge:Hg detectors matches well with the 10.6-micron radiation; however, when one considers the specific detectivity, $D*$ at 10.6 microns with, say, a narrow band 10.6-micron filter at the detector, the Ge:Cu and Ge:Hg detectors have about equal detectivities.

Table III. CHARACTERISTICS OF PHOTOCONDUCTIVE DETECTORS USABLE AT 10.6 MICRONS.

Material	Operating Temperature (Deg K)	Wavelength of Peak Response λ_p (microns)	Cut-Off Wavelength (50% Value)	D* (500°K,f,1) cm cps$^{1/2}$/watt	D* at λ_p
Ge:Au	77	5.0	7.5	6×10^9	1×10^{10}
Ge:Au	60	4.7	8.0	1×10^{10}	2×10^{10}
Hg:Cd:Te	77	11.5	12	$>5 \times 10^8$	$>5 \times 10^8$
Ge:Hg	30	11	13	8×10^9	1.5×10^{10}
Ge:Cu	<20	20	27	1×10^{10}	2.5×10^{10}
Ge:Cu:Sb	4.2	20	27	1×10^{10}	2.5×10^{10}
Ge:Zn	4.2	36	39.5	4×10^9	1×10^{10}

For the case of the gold-doped detectors, the detectivity for 10.6 microns is low, on the order of 10^8 cm cps$^{\frac{1}{2}}$/watt. Therefore, for a given operating condition, these detectors will have an S/N ratio of about 10^2 less than the Hg- or Cu-doped detectors. The main advantage of this detector, as well as the Hg:Cd:Te type, is that it can be operated at liquid nitrogen temperatures rather than liquid helium temperatures, drastically reducing the dewar complexity and operating costs.

The analysis in Section 2.6 has indicated that the desired frequency stability can be achieved with the use of the readily available Au:Ge detector operating at liquid nitrogen temperatures, if the control-loop bandwidth is limited to less than 100 Hz. Although this places a greater strain on the mechanical package as far as acoustical isolation is concerned, a great advantage of a much simpler detector is obtained. This is especially important when the unit is to be used in a relatively remote location.

Some work is progressing on improving the characteristics of the Hg:Cd:Te detector which also operates at liquid nitrogen temperatures. With new energy being put forth in the detector area, primarily because of the discovery of the 10-micron laser, detectors with much better characteristics over the Au:Ge may become available in the near future.

By analyzing the data from the manufacturer of the Au:Ge type of detector, it does not appear that the unit can be made to operate in the signal-shot-noise-limited condition even at input power levels for which saturation is expected to occur. Therefore, the detector itself is the major source of noise, and this noise is reflected in the quoted D* figures. For the Au:Ge detector, about the best available D* is 3×10^8 cm$\sqrt{Hz}$/watt at a wavelength of 10.6 microns for commercially available units. This corresponds to a noise equivalent power of 3.3×10^{-9} watts/cm$\sqrt{Hz}$. As long as the system is detector-noise limited, then the noise equivalent power of the system can be reduced by decreasing the area of the detector. Unfortunately, detector fabrication becomes extremely difficult for material sizes much smaller than $\frac{1}{2} \times \frac{1}{2}$ mm.

This size is not small enough to allow shot-noise-limited operation. However, it is encouraging to note that this size detector has a noise equivalent power of about 8.2×10^{-11} watts/$\sqrt{Hz}$ which is within an order of magnitude of the signal-shot-noise level for the expected maximum tolerable input laser power of about ½ milliwatt. It is conceivable, then, that by proper choice of detector parameters from fabrication to operating conditions, the Au:Ge may be able to be operated shot-noise-limited, thus reaching the ultimate sensitivity of the stabilization scheme.

The frequency response of most of the materials mentioned above is in the 10 MHz range or higher, depending on how they are doped. However, with the designs presently available on commercial dewars in which the detector is packaged, the frequency response is much reduced from the material value due to the stray capacitance associated with the dewar. For this particular application, where it is desired to have a modulation frequency in the 1 - 25 MHz range, but with bandwidths of only a few hundred cycles, resonant types of load circuits rather than resistive types can be used for the detector. The stray capacitance of the detector dewar can be used as part of the resonant circuit, allowing operation at higher modulation frequencies without loss in responsivity.

3.3   Optical Design

3.3.1   Introduction

The major components in the optical design for the stabilized CO_2 laser are the laser proper, the optical modulator, and the CO_2 amplifier. The optical design of the laser encompasses such areas as transverse mode control, wavelength selection, cavity mirror geometry, and coupling-out techniques. For the purposes of this program, the techniques which have been emphasized are those which would be capable of providing the maximum power output without degrading the mechanical rigidity of the laser cavity.

As discussed in the following sections, the optical modulator has been designed to provide the maximum phase deviation for a wavelength of 10 microns at a modulation frequency suitable for the optical detector. The material to be used is semi-insulating gallium arsenide. The CO_2 amplifier has been designed to provide the desired power gain of 2.0, while still maintaining long-term pressure and frequency stability.

The other optical components, being passive, have been designed in a very straightforward manner and will not be discussed in detail.

3.3.2 Laser Wavelength Control

The CO_2 laser can operate almost equally well on several different wave-lengths around 10.6 microns[6] depending on the rotational J value of the transition. Although the laser will generally only operate on one wavelength at a time, the choice of wavelength can be a random process depending on the length of the laser cavity and on which photon starts the lasing action. Once one transition begins oscillation, it "steals" atoms from all of the other rotational levels by fast Boltzmann relaxation among rotational levels. In many cases, for unstabilized lasers, as the laser mirrors vibrate and the axial modes shift in frequency, the laser oscillation jumps from one J transition to another, giving the appearance of multi-line operation. Figure 6 shows three Doppler curves associated with three possible transitions along with a possible set of cavity modes, drawn very much not to scale, in order to show how one line may have a cavity mode within its linewidth, while other lines do not.

For most normal laser lengths, the c/2L frequency spacing of the optical cavity is much greater than the CO_2 Doppler linewidth, $\Delta\nu_D$, given by

$$\Delta\nu_D = \frac{2\sqrt{2\ln 2}}{\lambda} \sqrt{\frac{kT_{mol}}{M}} \approx 50 \text{ MHz} ,$$
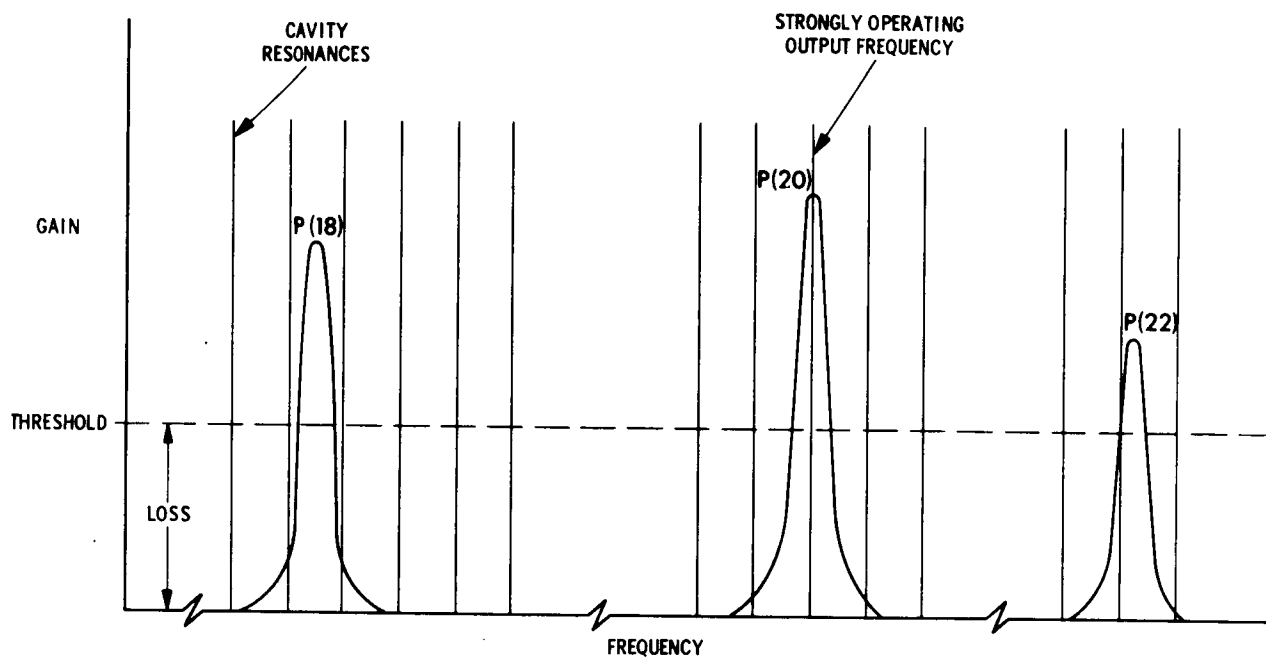
Figure 6. Single-Pass Gain versus Frequency for Three Lines of the CO_2 Laser, Showing Cavity Modes and P(J) Transitions.

where M is the molecular weight of the gas, T is the molecular temperature, k is Boltzmann's constant, and λ is the laser wavelength. The frequency spacing for the cavity resonances in the case of this program (L $\approx$ 50 cm) is about 300 MHz. However, there are so many possible J values which have positive gain (more than 50 have been measured[7]) that there may be several lines whose Doppler curves are simultaneously aligned with a cavity resonance. Chance circumstances then can dictate which line begins oscillation first. Although the cavity itself discriminates against a large number of wavelengths, further wavelength control is necessary to ensure that the laser will always operate on a fixed, predetermined wavelength.

In order to ensure that a cavity resonance is always under the Doppler gain curve of the desired output wavelength, from turn-on until after the warm-up period, the laser cavity must be temperature controlled to within about 1°C, when the cavity is made of invar. By thermal control, the unit can be made to always have a cavity resonance under the desired Doppler curve, but as mentioned above there may be several other Doppler curves which also fall on a cavity resonance. As observed in our laboratory, periodically a line of low gain will oscillate at high power, keeping the desired high gain line from oscillating. The laser can be turned off and then on again to get the required line.

To prevent operation on the undesired wavelengths, a wavelength selection device must be used either internal or external to the laser cavity. Several approaches are possible including internal cavity prism selection, internal or external grating selection, or another unique approach of a frequency-selective etalon which in principle may be used either internal or external to the laser cavity. An external prism will not normally have the resolution required to separate the CO_2 laser lines. It is not clear at this point which technique would be the most suitable for this application, although in principle they all should be effective in providing wavelength discrimination. However, because of practical considerations involving fabrication problems, material

41

quality and adaptability to the rigid, vibration-free cavity, the internal schemes do not appear too satisfactory. An external scheme with a grating or a frequency-selective etalon appears most promising when used in conjunction with a detector and automatic circuitry which can turn the laser on and off until the desired output wavelength is obtained. Because of space limitations, the frequency etalon approach appears most suitable.

The analysis and design of a frequency-selective etalon device, capable of discriminating between the various possible CO_2 laser wavelengths, follows very similar lines to that developed for the visible lasers for separation of the axial mode frequencies from a multi-mode laser. The similarity between the two cases lies in the regular frequency spacing between the various possible CO_2 laser wavelengths.

Within about ± 5 percent, the high-gain CO_2 laser wavelengths are separated in frequency by 52 GHz. It is possible to construct a high Q pass band cavity which will exhibit a periodic pass band configuration as shown in Figure 7. In this case when the cavity is tuned to transmit one wavelength, the other nearby wavelengths would be reflected since the cavity pass band repeats in only 48 GHz. Also, for the frequencies of interest, it is entirely possible to fabricate the device from a solid piece of optical material much the same as described by Peterson and Yariv[8]. Although their description and experiments were not directed toward this particular application, the analysis they present is entirely applicable.

The technique for fabricating a solid etalon is to polish a highly transparent piece of optical material to the desired etalon thickness, making sure that the material used is homogeneous and that the surfaces are very flat and parallel. By depositing non-absorbing multi-layer dielectric mirrors on either side of the etalon substrate, the bandpass characteristics can be achieved by the choice of mirror reflectivities.

The transmission of a lossless plane parallel etalon of length L, index of refraction n, and equal mirror reflectivities R is given by

$$\tau = \frac{1}{1 + [4R/(1-R)^2] \sin^2(2\pi nL \cos \theta/\lambda_0)} \quad , \tag{3.1}$$

where λ_0 is the free space wavelength of the incident radiation and θ is the angle between the incident refracted beam direction and the normal to the reflecting surface. The resolution, or finesse, F, which is the ratio of the frequency separation between successive transmission peaks, $c/2nL$, to the transmission bandwidth is given by

$$F = \frac{\pi R^{1/2}}{1-R} = \frac{c/2nL}{\Delta \nu} \quad . \tag{3.2}$$
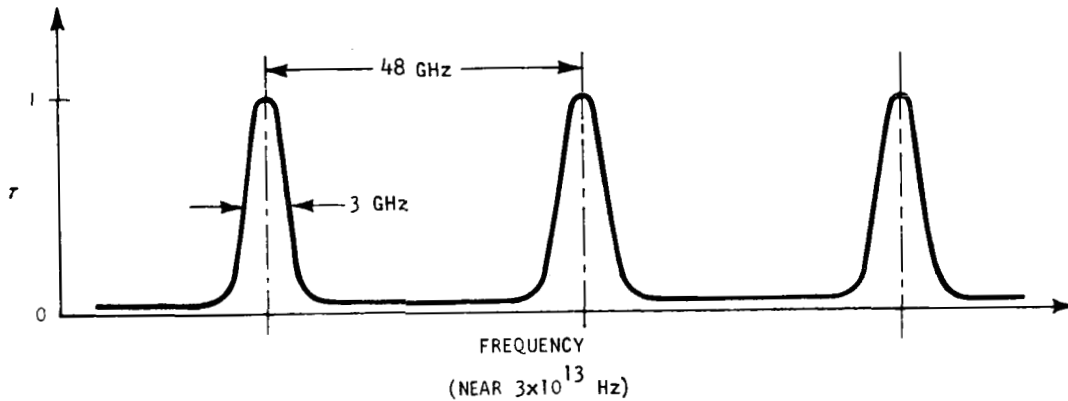
Figure 7. Pass Band Characteristics of a Short Fabry-Perot Etalon.

For wavelength selection in the CO_2 laser, the required finesse is about 48 GHz/3 GHz = 16. This corresponds to a reflectivity of about R = 82 percent, well within the range of multi-layer dielectric coatings at 10 microns.

An ideally manufactured device (no loss due to absorption or scattering and no reflectivity mismatch between mirrors) would have a periodic passband characteristic as shown in Figure 7. The transmission peaks would be 100 percent, and the transmission nulls would be near zero. As described by the above equations, the position of the transmission peaks in absolute frequency space is determined by the angle which the plate makes with the beam and the actual thickness of the plate. The wavelength for maximum transmission ($\tau = 1$) occurs when $2\pi nL \cos \theta / \lambda_0 = m$, or $\lambda_0 = 2nL \cos \theta / m$, where m is an integer 1, 2, 3, ...

The material which appears to be most ideally suited for use as the substrate is high purity germanium. In relatively low-power beams, it has negligible absorption at 10 microns, and can be polished very smooth and flat to act as an ideal mirror substrate.

Since germanium has an index of refraction of 4.00 at 10.6 microns, the thickness necessary to obtain the required $c/2nL$ spacing of 48 GHz is 0.78 mm.

Also, this device can be adjusted in angle θ to transmit the desired wavelength. Since for a germanium substrate 0.78 mm thick the value of m is about 300, the variation in θ to obtain a $\Delta m = 1$ (repeat of orders) is about $\pm 5^\circ$ around normal. At an angle of 2°, the angular adjustment for just tuning between the nearest two wavelengths ($\Delta \lambda \approx .02$ microns) can be calculated to be about 6 minutes of arc, a value which can be achieved easily with mechanical devices.

Unfortunately, the ideal passband characteristics cannot quite be met in such a device because of a small amount of loss which is inevitably

44

exhibited by the coatings and the substrate material due to absorption and scattering. For the 10-micron case, the scattering losses should be insignificant compared to the material absorption even though the absorption losses may be as low as one-half percent per pass. Therefore, losses can occur in the Fabry-Perot etalon primarily from two sources, absorption and reflectivity mismatch between surfaces. The transmission characteristics as a function of these variables are given as

$$\tau = \frac{(1 - a)T^2}{\left[1 - (1 - a)R\right]^2} \qquad \text{(transmission with absorption)} \qquad (3.3)$$

and

$$\tau = \frac{T_1 T_2}{(1 - \sqrt{R_1 R_2})^2} \qquad \begin{array}{l}\text{(transmission with reflectivity} \\ \text{mismatch) .}\end{array} \qquad (3.4)$$

For materials with no absorption $(a = 0)$ and for exactly equal reflectivities $R_1 = R_2$ and $T_1 = T_2$, $\tau = 1.0$.

Generally, coating procedures will not allow reproducibility of reflectivities closer than about ± 1 percent. T_1 and T_2 (therefore R_1 and R_2) can be as much as 2 percent different. Even with no absorption, the maximum τ for a mismatch in reflectivities of 2 percent at a reflectivity of about 82 percent would be about 99.5 percent. This reduction turns out to be small compared to the reduction in transmission due to absorption.

The reduction in peak transmission due to absorption can only be estimated since accurate information on the absorption coefficient in pure germanium and in the dielectric mirror coatings is not available. Estimates from measurements[9] which have been made indicate that total single-pass absorption in the etalon probably will not be greater than one-half percent. This amount of etalon loss will degrade the peak transmission to about 92.5 percent. Although this peak transmission will be satisfactory for use in a wavelength selector

external to the laser cavity, the device may not be applicable as an internal wavelength selector.

By placing the etalon in the portion of the laser beam tapped-off for the stabilization loop, the optical detector in conjunction with an automatic cycling system can be effectively used to search for the required wavelength. The etalon has the distinct advantage of being small and lightweight and does not require long optical path lengths to obtain the required resolution, a definite advantage over the grating or prism.

3.3.3 Laser Transverse Mode Control

For the case of the CO_2 laser, the gain of the laser transition is nearly independent of tube diameter, indicating the desirability of going to as large a diameter as possible as long as the mode volume can be utilized. Unfortunately, the diffraction losses for the higher-order modes go down as the tube diameter is increased so that the laser tends to oscillate in many high-order transverse modes. To fabricate a relatively short, stabilized tube and still maintain high output power, special techniques in cavity design need to be developed to utilize the large diameter characteristics of the CO_2 laser.

There are several techniques for suppressing unwanted transverse modes. These modes can exist in a laser even when its length is such as to allow only one longitudinal mode as in the case of the CO_2 laser. In almost all cases, however, the basic mechanism is to obtain differential loss between the TEM_{oo} mode and higher-order modes by diffraction. In the case of a laser, the lowest-order mode has a near Gaussian cross-sectional intensity distribution within the laser tube, i.e., with energy concentrated near the center of the tube. The higher-order modes progressively have more energy concentrated further from the center of the tube and are correspondingly affected more by the presence of the tube walls or the size of the mirrors or whatever the limiting aperture of the laser cavity happens to be.

It is possible to compute the losses incurred by each cavity mode for a particular choice of mirror curvatures and separation, tube diameters, and losses due to mirror transparency, absorption, and scattering. By choosing a mirror system so that the losses for all modes higher than TEM_{oo} are slightly greater than the laser gain, then only the lowest-order transverse mode will oscillate. It is therefore desirable to choose a cavity configuration that will provide as much discrimination in loss as possible between the first and higher-order modes of a cavity.

There are several techniques for accomplishing the selective mode loss in order to ensure lowest-order mode oscillation. Several most important examples are:

(1) Aperturing of the laser mode by introducing a limiting aperture into the laser cavity causing greater diffraction loss on the higher-order modes than on the lower[10]. By choosing the proper aperture size, the laser can be restricted to operate on the lowest transverse mode. This technique is used on most commercial lasers, but suffers in that in order to obtain large enough losses on the high-order modes to keep them from oscillating, the lowest-order mode experiences significant loss, reducing the maximum available output power.

(2) Choosing the curvature of the cavity mirrors such that the frequency separation of adjacent transverse modes is slightly greater than the Doppler linewidth[11]. This technique appears very applicable to short CO_2 lasers where the frequency separation between the cavity transverse modes can be made greater than 50 MHz. The disadvantage here is that the required mirror radius of curvatures is relatively small, overly restricting the diameter of the optical mode volume inside the laser cavity, thus limiting the laser power output capability.

(3) Utilizing an output coupling mechanism which draws the laser output
     from around the outside of a totally reflecting mirror, thus con-
     verting the power normally lost to diffraction into useful output.
     This technique appears to be most desirable for the case where
     maximum power output is desired from high gain lasers and, there-
     fore, has been designed into the stabilized CO_2 laser.

For the case of the CO_2 laser, the value of the tube diameter is not an
important parameter in the optimum gain of the tube and can be made large
enough to have no effect on the field distribution within the laser. By
making an output mirror with a small, totally reflecting spot deposited
on a transparent window, the laser output can be taken from around the spot.
The size of the spot would be chosen to provide the correct amount of feedback
to the laser cavity. Since the mode diameters of progressively higher-order
modes are increasing, thus moving their power densities to larger diameters,
the higher-order modes will not oscillate due to the large loss around the
output mirror. The mirror size is chosen to keep all but the lowest-order
mode from oscillating. Then all of the power in the lowest-order mode which
would normally have been wasted in diffraction losses is converted to useful
output.

In general, this technique of diffraction coupled output mirrors can
provide the greatest single-mode power output of any coupling scheme. Power
enhancements in high gain lasers by a factor of 10 have been observed over
conventional techniques[12]. Also, by making the mirrors with a large radius
of curvature, the mode volume can be made large while still maintaining good
mode discrimination. It is expected that total lowest-order mode sizes inside
the laser tube can be made about 12 mm in diameter using this technique on a
50 cm long tube.

Because of the blocking of the central part of the beam with the mirror
spot, a near field beam pattern will have a donut shape. The donut ring will

radiate by diffraction losses characteristic of its annular width, and a bright spot will periodically appear in the center of the donut as one moves away from the laser. This alternating center intensity effect disappears when one passes into the far field region of the beam and notices a Fraunhoffer diffraction pattern characteristic of an annular disc. The diffraction pattern from this type of output coupler is similar to that from the standard transparent mirror coupler where the diffraction pattern is determined by the diameter of the output beam, except that slightly more power is thrown into higher-order rings around the central maximum[13].

The beginning of the laser far field L_f can be estimated by the relation $L_f = D^2/\lambda$ where D is the effective output aperture, and λ is the operating wavelength. For the case of a CO_2 laser which emits a beam with an effective output diameter of 1 cm, the far field region starts in about 10 meters from the laser. For the stabilized CO_2 laser, the output mirror will have a totally reflecting spot of about 6 mm in diameter deposited on a suitable window material. The actual optimum size of the reflecting spot will have to be determined during the testing portion of the laser fabrication in order to achieve the condition for maximum power output.

Several tests were performed on this technique of diffraction output coupling and were compared with the conventional approach of multi-layer dielectric mirrors. A laser developed on the Sylvania Independent Research Program was used. The laser was 30 cm long with Brewster windows and had a bore diameter of 12 mm. Using a multi-layer dielectric mirror with 10 percent transmission, the multi-mode output power was about 3 watts. Placing a variable aperture inside the cavity and adjusting its diameter to obtain single transverse mode operation, a maximum power output of about 0.9 watts was achieved.

The multi-layer dielectric mirror was then replaced with a diffraction coupled output mirror which in this case had a 3 mm diameter gold spot placed

in the center of a potassium chloride window. The cavity mirrors were
optimally adjusted, and the laser gave a maximum single mode output power
of about 1.5 watts, substantially more than for the conventional approach.
The donut-shaped beam persisted for only about 20 cm before it started to
degenerate into a uniform output pattern.

The results of this effort have indicated the desirability of using
the diffraction coupled output mirror when maximum power is required in the
lowest-order transverse mode.

3.3.4   10.6-Micron Frequency Modulator

Any device which can phase or frequency modulate a CO_2 laser beam could
be used as a modulator for the stabilization loop. A vibrating mirror used
as one of the optical elements in the stabilization loop would provide quite
good phase deviations at the lower frequencies (less than 100 kHz), but at
higher frequencies, the electro-optic type of modulator is more able to give
the desired large phase deviations. At the present state-of-the-art in
commercially available liquid nitrogen-cooled detectors (see Section 3.2),
the modulation frequency f_m is limited by the detector to values in the low
MHz region. This is far below the maximum value of about 25 MHz limited by
the CO_2 Doppler line. However, higher values of f_m may be possible in the
near future as more and more emphasis is placed on the design of the dewars
which are used with the cooled detectors.

Therefore, the electro-optic type of modulator appears to be the most
desirable since its operational frequency is broadband and can be fit to any
value determined by other considerations of the scheme. Several electro-optic
phase modulators have been constructed[14,15] for use at 10.6 microns, all of
them being the GaAs type.

The peak phase delay (modulation index), δ, for radiation traversing
a GaAs crystal polarized along one of the birefringent axes is given by:

$$\delta = \frac{\pi \, n_0^3 \, r_{41} \, \ell V}{\lambda d} \, , \tag{3.5}$$

where n_0 is the index of refraction; r_{41}, the electro-optic coefficient; ℓ, the modulator length; V, the applied voltage; λ, the laser wavelength; and d, the modulator width.

The electro-optic coefficient for GaAs in the range 1.0 - 1.7 microns is given by Ho and Buhrer[16] as

$$n_0^3 \, r_{41} \approx 6 \times 10^{-6} \text{ cm/kv} \, . \tag{3.6}$$

More recent data at 10.6 microns (RCA Laboratories[14]) indicates that

$$r_{41} \sim 10^{-7} \text{ cm/kv}$$

$$n_0^3 \, r_{41} \approx 3 \times 10^{-6} \text{ cm/kv} \qquad (n_0 \approx 3.1) \, . \tag{3.7}$$

The latter value is probably more relevant to our problem.

Suppose that we use a modulator length ℓ which is double-passed (by placing a mirror at one end of the modulator); the total retardation will then be

$$\delta = \frac{2\pi n_0^3 \, r_{41} \, \ell V}{\lambda d} \, . \tag{3.8}$$

Putting in numerical values yields,

$$\delta \approx 0.02 \times \frac{\ell}{d} \times V(\text{kV}) \, . \tag{3.9}$$

The maximum length crystal which can be obtained in "semi-insulating" GaAs is about 8 cm long. The smallest practical width for passing the 10.6-micron

beam is about 3 mm. For this width, the maximum voltage which can be applied
before breakdown occurs is about 2 kv. These values give a maximum phase
deviation for a double-pass modulator of

$$\delta \; = \; 1 \; \text{radian peak.}$$

Since the modulator will be strictly a phase modulator, no analyzer or
quarter-wave plates are necessary; and since the laser will be made with
Brewster angle windows, the laser beam will automatically be polarized.

Figure 8 shows the assembly drawing of the modulator with all of the
vertical, horizontal, and rotational adjustments for alignment purposes.
The modulator crystal must be capable of being rotated around its optical
axis in order to accurately align the crystal birefringent axis with respect
to the 10.6-micron beam polarization plane. An external mirror is used to
fold the beam back on itself to obtain the double-passing advantage. The
modulator, along with its resonant driving circuit, will be placed into an
electrically-tight enclosure to eliminate the possibility of pick-up at the
detector.

3.3.5 CO_2 Amplifier

The CO_2 amplifier is one of the most critical components in the stabili-
zation scheme since the overall system stability is limited by the stability
of the gain curve exhibited by the CO_2 gas within the amplifier. In Section
2.7 the limits to this stability were discussed. It was found that frequency
shifts due to changes in the molecular collision processes between CO_2 and
itself or other gases is expected to be the primary cause of long-term absolute
frequency drift. Such effects as operating temperature changes in the amplifier
gas, or long-term pressure changes due, say, to gas clean-up or very small
vacuum leaks in the amplifier, or possibly variations in the discharge exci-
tation parameters, could cause substantial changes in the reference frequency
of the amplifier. The amplifier tube must, therefore, be designed and operated
for maximum uniformity of operating conditions over long periods of time.

Figure 8. Modulator Assembly.
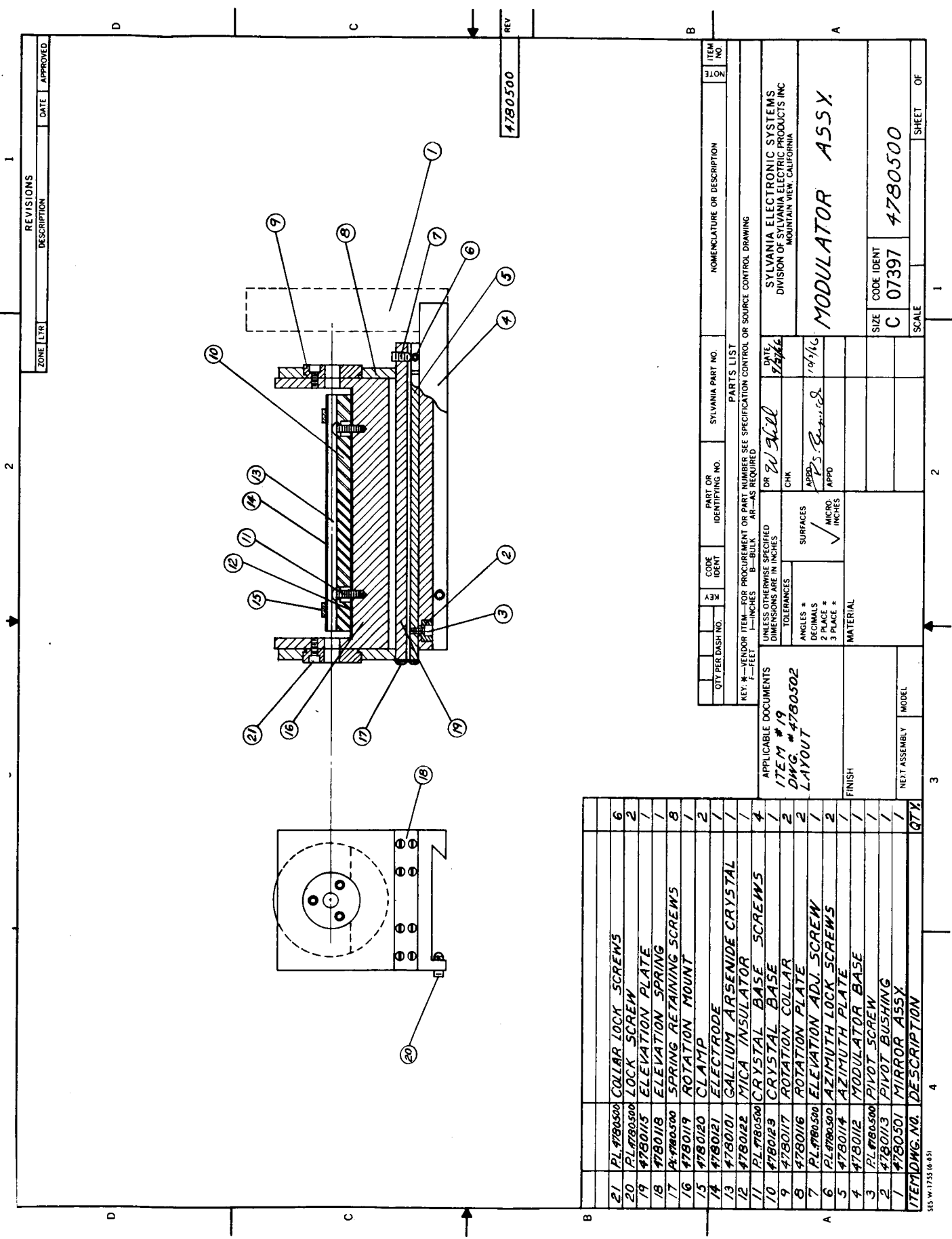
ITEM	DWG. NO.	DESCRIPTION	QTY
21	PL.4780500	COLLAR LOCK SCREWS	6
20	PL.4780500	LOCK SCREW	2
19	4780115	ELEVATION PLATE	1
18	4780118	ELEVATION SPRING	1
17	PL.4780500	SPRING RETAINING SCREWS	8
16	4780119	ROTATION MOUNT	1
15	4780120	CLAMP	2
14	4780121	ELECTRODE	1
13	4780101	GALLIUM ARSENIDE CRYSTAL	1
12	4780122	MICA INSULATOR	4
11	PL.4780500	CRYSTAL BASE SCREWS	1
10	4780123	CRYSTAL BASE	2
9	4780117	ROTATION COLLAR	2
8	4780116	ELEVATION ADJ. SCREW	1
7	PL.4780500	AZIMUTH LOCK SCREWS	2
6	4780114	AZIMUTH PLATE	1
5	4780112	MODULATOR BASE	1
3	PL.4780500	PIVOT SCREW	1
2	4780113	PIVOT BUSHING	1
1	4780501	MIRROR ASSY.	1

SYLVANIA ELECTRONIC SYSTEMS
DIVISION OF SYLVANIA ELECTRIC PRODUCTS INC
MOUNTAIN VIEW, CALIFORNIA

MODULATOR ASSY.

SIZE C   CODE IDENT 07397   4780500

APPLICABLE DOCUMENTS
ITEM #19
DWG. #4780502
LAYOUT

Although most of the information on the optimum excitation, gas fill conditions, and other similar parameters cannot be obtained until the device is constructed and tested, it is expected that the tube will operate at a fairly low total pressure of 1 - 3 Torr where any proportional changes in pressure will not have as large an effect on the reference frequency as at higher pressures. Also, when operated as a non-regenerative amplifier, this pressure range seems to be optimum for obtaining maximum gain. The excitation of the amplifier should be provided by an RF source operating at a frequency high enough to eliminate any measurable amplitude modulation on the beam. Any frequency greater than 5 MHz would be suitable. The RF technique of excitation does not require internal electrodes so that gas pumping due to chemical reaction or gas burial from sputtered electrode material cannot occur. This pumping effect due to internal electrodes has apparently been the major cause of limited lifetime in well-built dc-excited CO_2 laser tubes.

Little information has been published on the actual gain of the CO_2 amplifier when operated in a closed-off system, but from the information available[17], the maximum gain which probably can be achieved lies somewhere between 22 and 40 percent per meter. As seen in Section 2, the minimum frequency error which can be obtained depends inversely on the CO_2 amplifier gain function $G_o \ln G_o$ where G_o is the total amplifier gain. It is therefore extremely important to obtain as high a gain as possible from the CO_2 amplifier. Within the size limitations on the laser package (1 meter cube), the maximum active length which can be obtained for the amplifier is about 60 cm. To obtain the desired design number $(G_o = 2.0)$ suggested in Section 2, the amplifier cannot operate as a single-pass device, and some feedback would have to be provided by mirrors mounted at each end of the amplifier. The mirrors must be carefully chosen to provide maximum feedback without oscillation.

It appears that aperture-coupled mirrors will be suitable if the aperture size is constructed just large enough to prevent the amplifier from oscillating.

Using the available numbers for gain, two gold-coated mirrors with about 1.5 meter radius of curvature would be suitable if the input mirror aperture size is 2 mm in diameter and the output aperture size is about 5 mm in diameter. These numbers may vary slightly, depending on the actual gain characteristics of the RF-pumped amplifier. This three-pass, aperture-coupled technique will allow the attainment of an effective amplifier gain, G_o, of 2.0 in the 60 cm length, and possibly more, depending on the actual oscillation threshold characteristics of the amplifier. In order to make maximum use of the gain of the amplifier, the amplifier tube will be made with Brewster angle windows, matched in polarization to the CO_2 laser which is being stabilized. The quality of these windows must be quite good in order to keep any optical phase shifts small across the modulated beam.

In order to reach the gain figure mentioned above, the amplifier tube walls will have to be cooled to at least normal ambient temperatures. It may even be necessary to cool to lower temperatures with liquid refrigerants so as to increase gain and reduce the CO_2 Doppler linewidth (Δf_D), although only water cooling is presently anticipated.

3.4   Mechanical Design

3.4.1 Vibration Effects

Under normal environments, the laser output frequency, with its very narrow instantaneous spectral width, wanders in frequency due to changes in the relative optical position of the laser mirrors. When spectral width is measured in an experiment, these wanderings of the output frequency are averaged by the measuring instrument. The spectral width measured is a function of the amplitude and frequency spectrum of the mirror vibrations and the averaging time constant of the measuring instrument.

The lower limit to the extent of the frequency wandering can be predicted[18] from the thermal excitation of the lowest frequency longitudinal mode of the

laser cavity structure. For the type of cavities used on the stabilized CO_2 laser, the fundamental value for the vibration frequency stability is about

$$\left(\frac{\Delta f}{f}\right)_{\substack{thermal \\ vibration}} = 3 \times 10^{-15} \, ,$$

small compared to the desired stability of 1×10^{-10}.

If acoustical and mechanical vibration inputs to the structure have significant power at longitudinal mode frequencies of the structure, the magnitude of the wandering of the laser frequency will be increased. In addition, real laser structures may have elements with beam-like or plate-like geometries. Beams and plates have transverse vibration modes which may occur at quite low frequencies. Also, the joints between elements may have low-frequency modes. If any of these additional vibration modes occur at frequencies included in the power spectra of the acoustical and mechanical vibration inputs, the frequency wandering of the laser will be even further increased.

Although, under ultra-quiet laboratory conditions, lasers have been operated to within an order of magnitude of the theoretical thermal vibration limit[19], practical laser systems in normal laboratory environments are limited in their vibrational stability to much higher values. Table IV shows typical results of measurements made on the single-frequency He-Ne laser. The measurements made by Baird, et.al.[20,21] were with their own lasers. The measurements made by Targ[22] and Kerr[23] at Sylvania were with a commercial Spectra-Physics Model 119 laser.

Table IV. Summary of Experiments with Single-Frequency 6328Å He-Ne Lasers

Experimenter	$\frac{\Delta f}{f}$ vibration	Conditions
Baird et.al.	1.5×10^{-8}	Exp. laser in lab
Baird et.al.	3×10^{-10}	Exp. laser in lab
Targ	1.5×10^{-10}	#119 in Stand. lab
Kerr	1.5×10^{-11}	#119 in Best lab
Kerr	3×10^{-10}	#119 in Field

After considering the experimental results summarized in Table IV, it is concluded that it is definitely possible to fabricate a structure which is capable of providing the desired short-term stability of 1 part in 10^{10}, but much better acoustical shielding techniques than used in the past are most desirable.

3.4.2 Vibration Control

In order for a structure to be stable against vibration, it is necessary that the mechanical resonances of the structure not be at frequencies within the main power spectrum of acoustical and mechanical vibration noise inputs.

Acoustical noise and mechanical vibration noise are actually identical quantities, but we will define them as two separate noise sources. Acoustic noise will be defined as noise energy transferred as sound waves through the air, and mechanical vibration noise will be defined as noise transferred through the structural mounting.

The main power spectrum of both acoustic and mechanical vibration noise is at low frequencies. The peak of the acoustic spectrum usually occurs at less than 500 Hz. In both types of noise, however, there will be occasional shocks with frequency components of up to perhaps 30 kHz. The fact that most of the noise power spectrum for vibrational excitation occurs at low frequencies, together with the fact that high frequency noise is easier to isolate from a structure than is low frequency noise, dictates that the CO_2 laser structure should be designed to make the structural frequency resonances as high as can be achieved.

The frequency of the lowest longitudinal resonance of a laser cavity structure is determined by the cavity length. This frequency is given by the equation

$$f_{L\nu} = \frac{C_s}{2L} \tag{3.10}$$

where C_s is the velocity of sound in the structure, and L is the structure length.

In choosing a length for the CO_2 laser, one must make a trade-off between high longitudinal mode frequency and stiffness against bending distortion on the one hand and high output power on the other. Assuming a structure made of invar for thermal stability reasons, Table V shows the lowest longitudinal frequency for various cavity lengths.

Table V. Lowest Longitudinal Mode Frequencies in Invar Laser Cavities

Cavity Length	Frequency
1 m	2 kHz
50 cm	4 kHz
20 cm	11 kHz
10 cm	21 kHz

A 50 cm long cavity length was chosen for this program as being able to provide fairly substantial output power (about ½ watt single frequency) while still maintaining fairly high lowest-order resonant frequencies in the range where substantial vibrational damping can be applied.

The design of the remaining structure was then chosen to keep from lowering the basic first resonance. The individual elements of the structure were chosen with geometries and methods of support (boundary conditions) such that they do not have low frequency transverse resonances. The joints between the elements of the structure have also been considered. These joints were also designed so that they do not have any low frequency resonances. Especially critical are the joints perpendicular to the cavity length. One particularly good design for these joints is to use large contact areas under compressional stress. The spring constant of the joint will then be high. Designs with joints using only the spring force of a few screws to connect significant masses must be avoided.

The assembly design of the laser cavity is shown in Figure 9. The basic cavity without end plates is made from a single piece of invar and machined

Figure 9. Cavity Assembly.

CAVITY ASSEMBLY

SYLVANIA ELECTRONIC SYSTEMS
DIVISION OF SYLVANIA ELECTRIC PRODUCTS INC
MOUNTAIN VIEW, CALIFORNIA

SIZE	CODE IDENT	
D	07397	4780503
SCALE 1/1		SHEET

PARTS LIST

QTY	PART OR IDENTIFYING NO	NOMENCLATURE OR DESCRIPTION	ITEM NO
FULL	PL-4780503	POLYURETHANE FOAM	23
4	4780503	#4-40 x 3/8 FLATHEAD SCREWS	22
1	4780007	MIRROR RET. RING	21
6	PL-4780503	#0-32-1/8 ALLEN CAP SCREWS	20
8	4780111	END PLATE SHOULDER WASHERS	19
2	4780153	ELECTRODE EXT.	18
2	4780110	TUBE RETAINER-MT.	17
2	4780109	TUBE RETAINER-OUTER	16
2	4780109	TUBE RETAINER-INNER	15
1	4780510	TUBE ASSEMBLY	14
4	PL-4780503	4-40 ROSAN PRESS-NUTS	13
2	PL-4780503	4-40 7/8 PAN HEAD SCREWS	12
4	4780108	SHOULDER WASHERS	11
2	PL-4780303	4-40 LOCK WASHERS	10
2	4780057	KCL BREWSTER WINDOWS	9
1	4780056	KCL BREWSTER MIRROR	8
1	4780055	10 METER SPHER MIRROR	7
1	4780157	PIEZO-ELECT DRIVE	6
1	4780106	MIRROR ADJ PLATE - OUTPUT	5
1	4780105	MIRROR ADJ PLATE - PIEZO	4
1	4780104	CAVITY END PLATE	3
1	4780103	CAVITY BODY	2

NOTE

BEAM OFFSET .085"
BEAM HEIGHT 2.062"
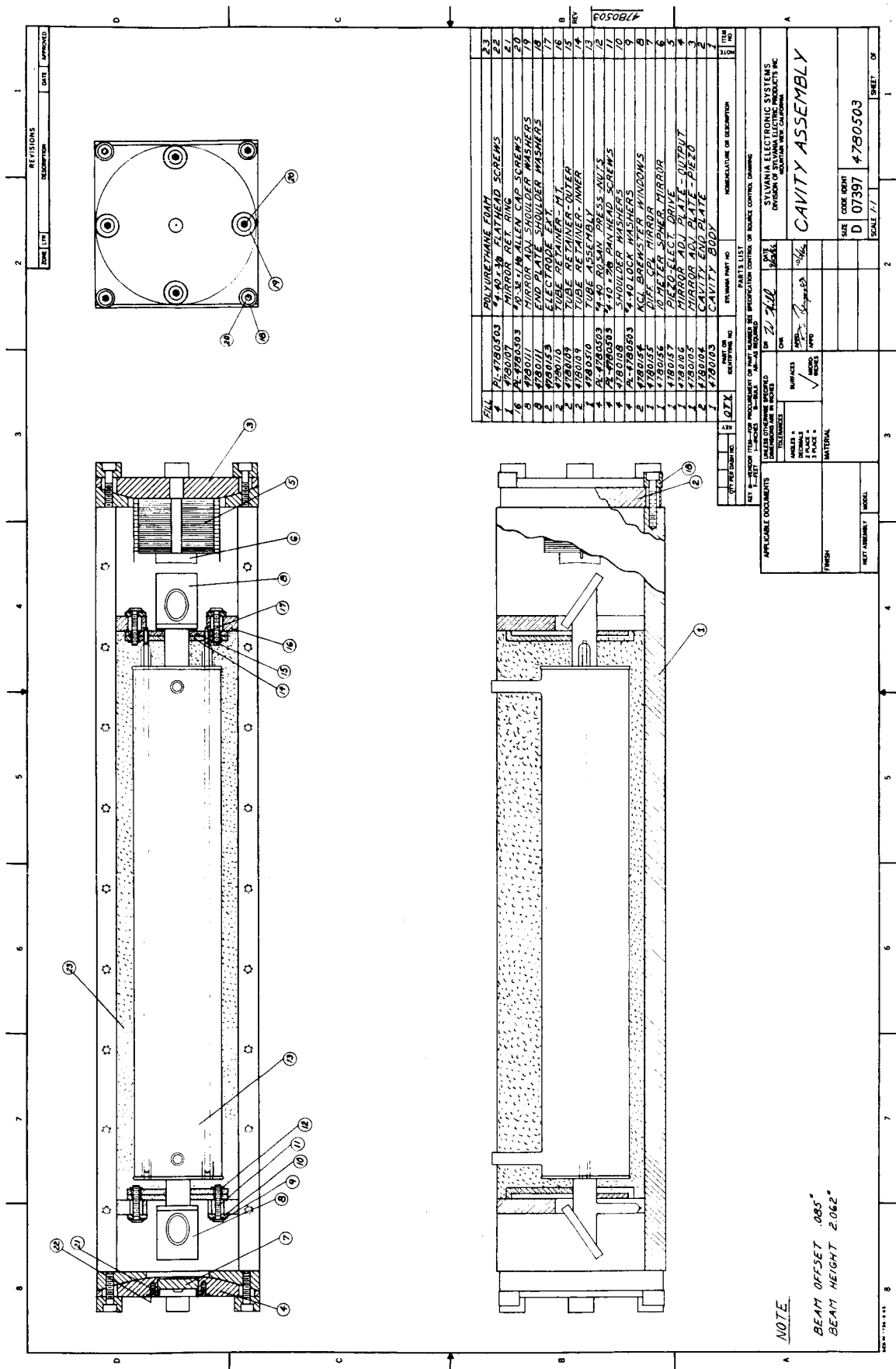
REVISIONS

to form a U-shaped member. The choice of a single block of material was made in an attempt to ensure equal coefficient of expansion throughout the material. A top plate will be bolted on after assembly in order to achieve the required stiffness of a rectangular structure. The end plates, also made of invar, are each made from two plates, their mating surface cut to a long radius. This provides the capability of a small angular adjustment of the mirror attached to the outer plate without the necessity of springs or other vibration-prone joints. After the mirrors are aligned, the end plates can be tightly clamped to the cavity U-shaped structure.

The laser tube mounting structure has been designed so that the tube locating mount (Item 16 in the drawing) can be removed after the tube has been potted in plate. The tube will only contact the cavity structure through the foam potting material, further isolating the cavity from any outside connections to the tube. An electrical heater will be placed within the cavity area to maintain the temperature of the cavity to within one degree celsius. The entire unit will be acoustically isolated by laminate structures from the rest of the stabilized CO_2 laser package. Also, to reduce the effects of air convection and variations in the index of refraction in the region between the Brewster windows and mirrors, dust covers will be used in this area. These are not shown on the drawing.

Even after designing a laser structure with only damped high frequency resonances, it is still necessary to provide acoustic and vibration noise isolation in order to achieve 1 part in 10^{10} frequency stability. The traditional method of achieving such isolation is to mount the laser cavity in a box lined with acoustical padding and to support the mass of the box and laser on a series of damped low spring constant springs.

Acoustical padding techniques are perfectly acceptable methods of isolating against acoustic noise and have been used extensively in the present design. However, the main problem associated with using a damped spring isolator for mechanical vibration noise isolation is that the angular and spatial position

of the laser beam with respect to a base plane is very erratic and indeter-
minant. Such a situation is unacceptable for many applications (especially
field applications), and alternate techniques have been devised to mechanically
stabilize the laser mounting structure.

A mechanical vibration noise isolator which does maintain rigid alignment
of the laser beam with respect to the base can be made with a series of "layered
media." The acoustical impedance of each layer is chosen so that a large im-
pedance mismatch occurs at each interface. This causes large reflection of
acoustic waves at the interfaces. The materials in the layers are further
chosen to produce high acoustic wave absorption coefficients.

The net result is that mechanical vibration noise energy which must go
through the "layered media" in the form of acoustic waves is reflected by the
series of interfaces and the energy is absorbed in the layers. This is achieved
while maintaining rigid alignment of the laser beam with respect to the base.

In addition to the "layered media" isolation at the bottom, the laser
structure must be completely enclosed on the top and all four sides with a
box containing acoustic damping material. It is also desirable that the top
and sides of this box be made with sandwich construction so that they will be
heavily damped and not resonate. A laminate structure consisting of layers
of magnesium and linen-base phenolic bonded together by Hysol type 0266 epoxy
appears to have the required properties.

Also, extreme care must be made in the choice of components to be used
near or within the laser structure which could be a source of vibration energy.
A constant flowing gas system for the CO_2 laser would not be tolerable because
of the vibration problems associated with a mechanical vacuum pump. Also, the
frequency modulation scheme to be used within the laser structure should be
electro-optic in nature as is planned for this program. A modulation scheme
utilizing an oscillating mirror, which may be acceptable from the electronic
point of view, would be a source of vibration which would be difficult to
counteract.

61

3.4.3 Thermal Control

Since the laser system will be utilizing an electronic control feedback loop which will track any laser frequency changes occurring at rates from dc to about 100 Hz, the extent of the thermal control will be strictly to keep the dc drift within the limits of the control system. By utilizing invar as the cavity material and controlling its temperature with a simple sensing unit, the objectives can easily be met.

The coefficient of expansion of free machining invar is about $1.0 \times 10^{-6}/^{\circ}C$ for temperatures near ambient. With a simple thermal control unit, temperature control to within $1^{\circ}C$ is easily obtained, giving a range in length variation of the cavity, $\Delta L/L$, of 1 part in 10^6. To compensate for this amount of cavity length change, the piezoelectric transducer used in the control loop will have to be capable of a ½-micron movement for the 50 cm long laser cavity. This value is not excessive for a piezoelectric "stack" or "capadyne" where a series of piezoelectric plates are stacked to give series mechanical movement but parallel electrical connections. These units can be made very rigid by epoxy potting techniques for use in systems where vibration effects are a problem.

3.5 Electronic Design

The primary objective of the control system is to stabilize the frequency of the main CO_2 laser oscillator. To accomplish this objective, a closed-loop frequency control scheme is used to minimize the FM distortion by controlling the cavity length of the main laser oscillator with piezoelectric tuning.

The frequency stabilization requirement of 1 part in 10^{10} demands an ultra-high system sensitivity. The attainment of the objective hinges upon development of a very low noise and low ripple, high gain, drift-free, and stable system which can react to minute input perturbations within the system signal spectrum and performs the appropriate frequency corrections. The following sections describe the components of the stabilization networks in detail with reference to Figure 10, the system block diagram.
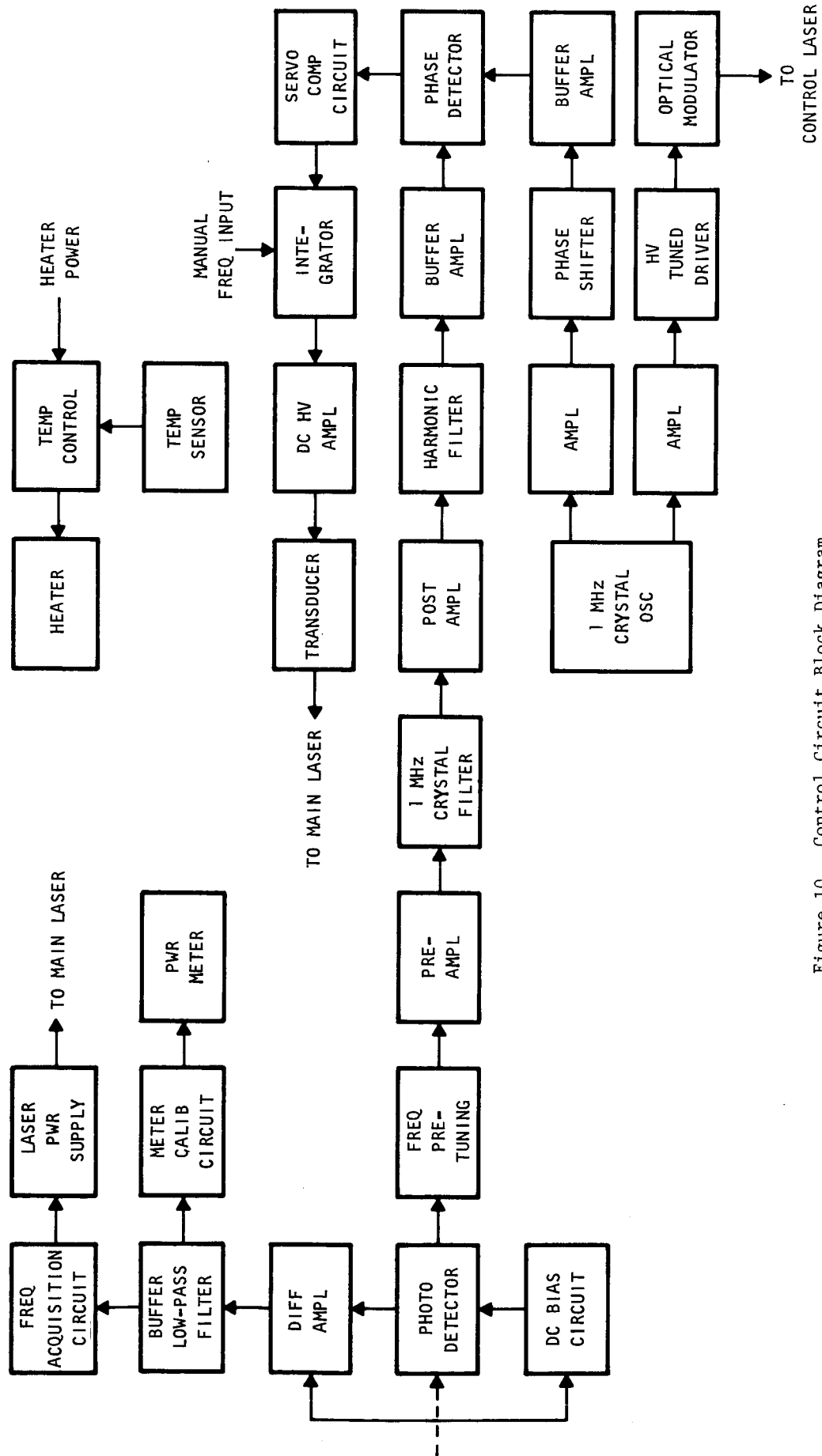
Figure 10. Control Circuit Block Diagram

63

3.5.1 Bandpass Amplifier

A preamplifier-bandpass filter-postamplifier configuration has been selected for this bandpass amplifier. The amplifier must be of a very high-gain, low-noise type at the carrier frequency of 1 MHz and have sufficient off-frequency rejection to reduce amplitudes of undesirable signals appearing in the vicinity of the spectrum of interest.

Since the calculated input signal level of the amplifier is approximately -130 dbm, the gain required of the amplifier is 147 db. To amplify the input signal to a level suitable for the 1 MHz crystal filter, a voltage gain of approximately 129 db is necessary. This gain is provided by two stages of cascaded field effect transistor amplifiers and eight additional stages of Amelco type E13-511 integrated videoamplifiers. The field effect transistor input stages are chosen because of superior low noise and high input impedance characteristics. The two stages of the field effect transistor amplifier produce a gain of 40 db. The postamplifier, two stages of Amelco E13-511 integrated videoamplifiers, furnishes the required remaining gain of 18 db plus a gain corresponding to 6 db insertion loss of the crystal filter.

The degree of frequency tuning the bandpass amplifier is allowed to perform is entirely governed by the amount of phase shift the sideband signals experience. Although from the noise standpoint, the bandpass amplifier is desired to have as narrow a passband as possible, the effect of the sharp tuning upon the sideband phase shift jeopardizes stability of the control system. The primary frequency tuning is accomplished by a two-crystal 1 MHz Butterworth filter with a 3-db bandwidth of 3 kHz. This filter is chosen chiefly because of its relatively linear envelope delay and passband characteristics.

The secondary frequency tuning is made at two points in the bandpass amplifier. At the input of the preamplifier is a parallel LC circuit tuned to 1 MHz. The tank circuit discriminates unwanted wideband noise from the signal perturbations entering the preamplifier. A variable capacitor together

with the input capacitance of the field effect transistor is used to tune to the inductor at the carrier frequency. At the output of the postamplifier is another LC tank circuit tuned to the second harmonic of the carrier frequency. The circuit removes possible harmonic distortion contained in the signal being fed to the phase detector.

A Darlington connected buffer circuit at the output of the postamplifier provides a high impedance load to the amplifier and also serves as an impedance matching network for the 50-ohm input impedance of the phase detector.

Low noise metal film resistors, high-Q ferrite core inductors, etc. are used in the critical portions of the bandpass amplifier to obtain its required performance.

3.5.2 Phase Detector

The phase detector is a Model 10514 Double Balanced Mixer manufactured by Hewlett-Packard Company. The unit has a conversion loss of 6 db, noise figure of approximately 8 db, and an input and output impedance of 50 ohms. The phase detector is a transformer-coupled, fullwave-bridge, rectifier circuit. Its dc coupled output feature and superior balance characteristics make the device suitable for this application.

The phase detector receives a reference signal from the 1-MHz crystal oscillator and a perturbation signal from the bandpass amplifier. The output of the phase detector is a low-frequency error signal whose amplitude is proportional to the cosine of the phase difference between the reference and the perturbation signals.

3.5.3 DC Amplifier Circuit

The dc amplifier circuit consists of a low-pass filter/servo-compensator, an integrator, and a dc high voltage amplifier.

The low-pass filter/servo-compensator is an active RC network built
with a molded operational amplifier and RC networks. The servo-bandwidth
is limited to approximately 100 Hz. The servo-compensating network modifies
the frequency response characteristics of the stabilization control system
to ensure at least 30 degrees of phase margin. The integrator is formed with
a molded operational amplifier and a feedback capacitor. An adjustable dc
voltage can be fed into the second input of the integrator for manually ad-
justing the frequency when it is necessary. The operational amplifiers used
in the circuit are Model D-9 molded case operational amplifiers manufactured
by Data Device Corporation.

The dc high voltage amplifier is a KEPCO Model ABC-1000M programmable
power supply. An external variable voltage, namely the integrator output
voltage, serves as a program source for the power supply which has the maximum
gain of 80 db and rms ripple of 1 millivolt. To drive the piezoelectric crystal,
which appears as a capacitive load, without causing an instability, decoupling
of the power supply from the load with a resistance equal to the output im-
pedance of the power supply is absolutely necessary. To ensure long-term
stability of the laser, the dc high voltage amplifier must have a very large
output voltage range since the thermal drift of the laser frequency is basi-
cally monotonic. A range from zero to 1000 volts is provided by this unit.

3.5.4 1-MHz Crystal Oscillator Circuit

The 1-MHz oscillator which generates the reference signal for the phase
detector and the driving voltage for the optical modulator is a modified
Miller oscillator using a field effect transistor. The high input impedance
of the field effect transistor in parallel with the 1-MHz crystal does not
reduce the effective Q of the circuit. A source follower circuit following the
oscillator reduces the output impedance of the circuit.

The variable phase-shifter provides a necessary adjustment of phase angle
of the oscillator output signal with respect to that of the error signal in

order to account for any phase shift the error signal may experience in the control system. A Darlington circuit at the output of the phase-shifter serves as a buffer as well as an impedance matching network for the 50-ohm input impedance of the phase detector.

3.5.5 Optical Modulator Driver

The optical modulator driver receives its input signal from the 1 MHz crystal oscillator. A ferrite core transformer performs a necessary impedance transformation at the input of the driver. The input stage of the driver circuit is a Class A transistor amplifier which supplies necessary power to the driver. The driver is an LC tank circuit with a high effective Q. The values of the inductor and the capacitor, including the input capacitance, etc. of the optical modulator, are chosen such that the tank circuit resonates at 1 MHz. Amplitude of the ac driving voltage generated across the tank circuit at the resonant frequency is a product of the output voltage of the Class A amplifier and the effective Q of the circuit. An effective Q of 125 and 16 volts rms output from the Class A amplifier produce the required 2 kilovolts driving voltage for the optical modulator.

3.5.6 Frequency Acquisition Circuit

Since the CO_2 laser can and does operate on several different wavelengths in the vicinity of 10.6 microns, it is necessary to restrict the CO_2 laser oscillation to only one preselected frequency, for a fixed frequency oscillation of the laser is essential in a heterodyne system.

A wavelength selection technique used in the CO_2 laser system prevents the laser beam from being directed to the photodetector when the CO_2 laser is operating at a wrong frequency. The presence of the correct laser wavelength permits a current conduction through the photodetector. DC voltage variations across a sensing resistor in the dc biasing circuit of the photodetector are amplified by a chopper-stabilized high gain differential amplifier

67

and fed to a gate circuit of the frequency acquisition circuit. Absence of this dc voltage causes generation of a series of 2-Hz rate pulses which in turn resets and restarts the laser power supply. A transistor gate circuit, a unijunction transistor relaxation oscillator with a buffer amplifier accomplish the above function. The frequency acquisition circuit continues to function until the laser oscillates at the correct frequency.

The dc voltage variation across the sensing resistor is also used to indicate the output power level of the laser. An operational amplifier scaling circuit provides a necessary readout calibration of a power meter.

3.5.7 Temperature Control

The temperature within the laser enclosure is controlled by a dc temperature control circuit. A temperature-sensing thermistor used in one leg of a balanced bridge circuit produces an unbalanced condition in the bridge circuit when the enclosure temperature deviates from the set point. A chopper-stabilized dc differential amplifier amplifies the unbalanced potential caused by the thermistor, and provides an input to a two-stage transistor driver. A heating coil connected between a dc heater power supply and collectors of the driver transistors generates heat as demanded by the sensor. A potentiometer at the input of the driver provides a temperature adjustment for the circuit. Since the heater will be located near the invar cavity mount, the heater dc supply will be well filtered so that low frequency magnetostrictive effects exhibited by the invar cannot be excited.

4.   SUMMARY AND RECOMMENDATIONS

Based on the analysis presented in the previous sections, it appears
possible to fabricate a CO_2 laser which will have the desired frequency
stability of 1 part in 10^{10} by using an active stabilization scheme
involving an external non-regenerative CO_2 amplifier. Furthermore, it
appears that the goals can be met with present state-of-the-art
components.

The external amplifier serves as a reference source to which the laser
frequency is stabilized. In the stabilization scheme, a small portion of the
laser output is shunted to an FM modulator which places FM sidebands on the
shunted beam. The beam is then passed through the CO_2 amplifier which
distorts the FM spectrum slightly. The beam is then directed to a photo-
conductive detector. When the laser frequency is off the center of the
amplifier frequency, a beat note appears at the detector which can be used
as an error signal. The amplitude of the beat signal goes to zero as the
laser frequency approaches the center frequency of the amplifier. The
limit to the sensitivity of the scheme is fixed by the noise level of the
stabilization loop, and with presently available liquid nitrogen-cooled
detectors, it appears that the detector itself is the major source of noise
in the system.

To reach the goal of a stability of 1 part in 10^{10}, the electronic
stabilization scheme will have the following parameters.

    a.   Servo-loop bandwidth to be 100 Hz or less (limited by system
        noise).

    b.   Modulation frequency of external modulator to be $\geq$ 1 MHz.

    c.   Frequency modulation index to be greater than, or equal to, unity.

    d.   The effective single-pass amplifier length is to be $\geq$ 1.8 meters.

The above requirements are based on the use of existing liquid nitrogen-cooled, gold-doped germanium detectors, chosen for highest D* at 10.6 microns.

Since the electronic stabilization network will be limited to tracking laser frequency fluctuations which occur at rates of less than 100 Hz, it will be necessary for the mechanical package to essentially eliminate all vibrational influences which occur at frequencies higher than 100 Hz. Specialized techniques involving multilayered baffling will be necessary, but information gained from stability measurements on the He-Ne laser indicate that the desired results can be achieved.

To maintain high sensitivity, the modulation frequency should be chosen as high as the detector will allow, to a limit of about 20 MHz. The use of an electro-optic type modulator such as GaAs appears to be most suitable, especially if an extension to greater stability levels is desired in the future. Although not readily available, these modulators have been demonstrated to work well at 10.6 microns.

In order to reduce the noise on the laser beam and increase tube life, rf excitation techniques should be used for both the laser tube and the amplifier tube. The laser tube should be filled to an appropriate pressure utilizing a mixture of CO_2, N_2, and He for maximum output power. The amplifier should be filled to an appropriate pressure and gas composition to provide for a maximum single-pass gain and pressure stability. The best operating conditions for the amplifier have not yet been determined and need to be examined during the course of the amplifier fabrication. Since heterodyne operation between two such lasers is contemplated, the CO_2 amplifiers for both lasers should be made and processed simultaneously. Unequal internal pressures can result in relatively large differences in output frequency (a few MHz per Torr, typically). Fortunately, the effects of external magnetic fields and electric fields on the frequency stability of the laser will be negligible.

The cavity length for the laser should be chosen as long as possible, for highest output power, without running into mechanical resonance problems. A cavity length of about 1/2 meter seems to be a reasonable compromise. This cavity length should allow single-frequency power output levels on the order of 1/2 watt.

The CO_2 laser is capable of operation on many wavelengths, although only one at a time; and since heterodyne experiments will be performed with the laser, wavelength control and selection will be necessary. The technique for choice of a particular line can be accomplished in many ways, but no one technique appears to be outstanding. Wavelength control by frequency-selective etalon techniques appears to be most suitable for this application.

The technique which appears most suitable for higher order mode control utilizes a diffraction coupled output mirror. This technique allows mode control without restricting the power output capabilities of the laser.

Standard control-loop techniques can be used in the servo-control system and will not be a limiting factor in the operation of the system. Loop bandwidths on the order of 5 to 10 kHz are possible and can be utilized when better liquid nitrogen-cooled optical detectors become available.

A detailed mechanical and electrical design for the laser has been completed, and the major design areas have been discussed in the earlier sections. The required size of the laser with the optical stabilization components is 100-cm long by 35-cm wide by 20-cm high without the power supply.

It is recommended that the stabilized laser utilizing the external CO_2 amplifier stabilization technique be constructed and tested using the readily available gold-doped germanium detector. Once the system has been evaluated, and it is definitely shown that the system is being detector limited, then consideration can be given toward the possibility of replacing the Au:Ge detector with a more suitable detector, if available.

71

5. REFERENCES

1. A. D. White, "Frequency Stabilization of Gas Lasers," _IEEE Journal of Quantum Electronics_, Vol. QE-1, November 1965, p. 349.

2. W. R. Bennett, "Mode Pulling in Gas Lasers," _Quantum Electronics III_, P. Grivet and N. Bloembergen, Eds., Columbia University Press, New York, 1964, p. 441.

3. W. R. Bennett, S. F. Jacobs, J. T. Latourette, and P. Rabinowitz, "Dispersion Characteristics and Frequency Stabilization of a Gas Laser," _Applied Physics Letters_, Vol.5, August 1964, p. 56.

4. A. D. White, E. I. Gordon, and E. F. Labuda, "Frequency Stabilization of Single Mode Gas Lasers," _Applied Physics Letters_, Vol. 5, September 1964, p. 97.

5. E. T. Gerry and D. A. Leonard, "Measurement of the 10.6 Micron CO_2 Laser Transition Probability and Optical Broadening Cross Sections," _Applied Physics Letters_, Vol. 8, 1 May 1966, p. 227.

6. C. K. N. Patel, "Interpretation of CO_2 Optical Maser Experiments," _Physical Review Letters_, Vol. 12, No. 21, May 1964, pp. 588-590.

7. G. Moeller and D. Rigden, "Observation of Laser Action in the R-Branch of CO_2 and N_2O Vibrational Spectra," _Applied Physics Letters_, Vol. 8, No. 3, February 1966, pp. 69-70.

8. D. G. Peterson and A. Yariv, "Interferometry and Laser Control with Solid Fabry-Perot Etalons," _Applied Optics_, Vol. 5, June 1966, p. 985.

9. Data from Optical Coating Laboratories, Inc., Santa Rosa, California.

10. T. Li, "Diffraction Loss and Selection of Modes in Maser Resonators with Circular Mirrors," _Bell System Technical Journal_, Vol. 45, May 1965, p. 917.

11. J. P. Goldsborough, "Beat Frequencies between Modes of a Concave-Mirror Optical Resonator," _Applied Optics_, Vol. 3, February 1964, p. 267.

12. J. T. Latourette, S. F. Jacobs, and P. Rabinowitz, "Improved Laser Angular Brightness through Diffraction Coupling," _Applied Optics_, Vol. 3, August 1964, p. 981.

13. M. Born and E. Wolf, _Principles of Optics_, MacMillan Company, New York, 1964, p. 328.

14. T. E. Walsh, "Gallium-Arsenide Electro-Optic Modulators," _RCA Review_, No. 39354, June 1966.

15. A. Yariv, C. A. Mead, and J. V. Parker, "GaAs as an Electro-Optic Modulator at 10.6 Microns," _IEEE Journal of Quantum Electronics_, Vol. QE-2, August 1966, p. 243.

16. L. Ho and C. F. Buhrer, "Electro-Optic Effect of Gallium Arsenide," _Applied Optics_, Vol. 2, June 1963, p. 647.

17. R. Farreng, et.al., "Amplification du rayonnement d'un laser a CO_2 par du gaz carbonique excité en haute frequence," <u>C. R. Acad. Sc. Paris</u>, Vol. 261, 4 October 1965, p. 2617-2620.

18. A. E. Siegman, et.al., "Laser Material (Spectroscopy)," Semi-annual Report No. 2 (June 15, 1965 - December 15, 1965), Contract DA 28-043-AMC-00446(E), U. S. Army Electronics Command, Fort Monmouth, New Jersey. M. L. Report No. 1401, Microwave Laboratory, W. W. Hansen Laboratory of Physics, Stanford University, California.

19. T. S. Jaseja, A. Javan, and C. H. Townes, "Frequency Stability of He-Ne Masers and Measurement of Length," <u>Physical Review Letters</u>, Vol. 10, No. 5, March 1963, p. 165-167.

2C. K. M. Baird, D. S. Smith, G. R. Hanes, and S. Tsunekane, "Characteristics of a Simple Single-Mode He-Ne Laser," <u>Applied Optics</u>, Vol. 4, No. 5, May 1965, p. 569-571.

21. D. S. Smith, K. M. Baird, and W. E. E. Berger, "Electrodeless Excitation of He-Ne Gas Lasers," <u>Applied Optics</u>, Vol. 4, No. 12, December 1965, p. 1673.

22. Russell Targ, private communication.

23. J. R. Kerr, "Microwave Optical Receiver Techniques," Technical Report No. AFAL-TR-66-254, Contract AF 33(615)-3108, June 1966, Sylvania Electronic Systems, Mountain View, California.

Appendix A
EVALUATION OF THE FUNCTION K(ᾶ)

We have defined the function

$$\tilde{K}(\tilde{\alpha}) \equiv \int_{-\infty}^{\infty} \frac{1}{\tilde{\alpha} - jy} e^{-y^2} dy$$

In general, this function cannot be evaluated in any simple form. However, the following expansions do exist.

For large values of $\tilde{\alpha}$ one can expand the first term in the integrand in a Taylor series in powers of $y/\tilde{\alpha}$, and then integrate this series term by term. The result is

$$\tilde{K}(\tilde{\alpha}) \approx \frac{\sqrt{\pi}}{\tilde{\alpha}} \left[1 + \sum_{n=1}^{\infty} \frac{1 \cdot 3 \cdot 5 \cdots (2n - 1)}{(j\sqrt{2} \ \tilde{\alpha})^{2n}} \right] \qquad |\tilde{\alpha}| \gg 1$$

It is important to note, however, that this series is only <u>asymptotically convergent</u>. That is, for any large value of $|\tilde{\alpha}|$ this series will at first converge as additional terms are included. If too many terms are taken, however, the factor $1 \cdot 3 \cdot 5 \cdot \ \cdots \ (2n - 1)$ in the numerator will eventually become larger than the denominator, and the series will begin to diverge as still more terms are included. Hence, the above expansion must be applied with care.

Useful series expansions for small $\tilde{\alpha}$ can be obtained as follows. An integral expression for $d\tilde{K}(\tilde{\alpha})/d\tilde{\alpha}$ can be obtained by differentiating with respect to $\tilde{\alpha}$ inside the integral for $\tilde{K}(\tilde{\alpha})$. An integration by parts on the $d\tilde{K}(\tilde{\alpha})/d\tilde{\alpha}$ integral will then yield the differential equation.

$$\frac{d\tilde{K}(\tilde{\alpha})}{d\tilde{\alpha}} = 2\tilde{\alpha}\tilde{K}(\tilde{\alpha}) - 2\sqrt{\pi}$$

Let $\tilde{K}(\tilde{\alpha}) = \exp(\tilde{\alpha}^2)\ \tilde{L}(\tilde{\alpha})$. Then

$$\frac{d\tilde{L}(\tilde{\alpha})}{d\tilde{\alpha}} = -2\sqrt{\pi}\ \exp(-\tilde{\alpha}^2)$$

Integrating both sides of this, and using the fact that $\tilde{K}(o) = \tilde{L}(o) = \pi$, gives

$$\tilde{L}(\tilde{\alpha}) = \pi - \int_{o}^{\tilde{\alpha}} 2\sqrt{\pi}\ e^{-t^2}\ dt$$

But, the definition of the error function, erf z, is

$$\operatorname{erf} z \equiv \frac{2}{\sqrt{\pi}} \int_{o}^{z} e^{-t^2}\ dt$$

Hence, we obtain

$$\tilde{K}(\tilde{\alpha}) = \pi \exp(\tilde{\alpha}^2)\ [1 - \operatorname{erf} \tilde{\alpha}]$$

Abramowitz and Stegun* give the series expansions

$$(7.1.5)\quad \operatorname{erf} \tilde{\alpha} = \frac{2}{\sqrt{\pi}} \sum_{n=o}^{\infty} \frac{(-1)^n\ \tilde{\alpha}^{2n+1}}{n!\ (2n+1)}$$

$$(7.1.6)\quad \operatorname{erf} \tilde{\alpha} = \frac{2}{\sqrt{\pi}} \exp(-\tilde{\alpha}^2) \sum_{n=o}^{\infty} \frac{2^n \tilde{\alpha}^{2n+1}}{1 \cdot 3 \cdots (2n+1)}$$

By using either of these equations for small values of $\tilde{\alpha}$, together with the asymptotically convergent series given above for large $\tilde{\alpha}$, we obtain the asymptotic expressions:

---

*Milton Abramowitz and Irene Stegun, <u>Handbook</u> <u>of</u> <u>Mathematical</u> <u>Functions</u>, Dover Publications.

$$K(\tilde{\alpha}) \approx \begin{cases} \pi - 2\sqrt{\pi}\,\tilde{\alpha} \quad , & \tilde{\alpha} \to 0 \\[2ex] \dfrac{\sqrt{\pi}}{\tilde{\alpha}} & \tilde{\alpha} \to \infty \end{cases}$$

The small $\tilde{\alpha}$ approximation is used in Section 2-4 of the text.